Vertical observations of the atmospheric boundary layer structure over Beijing urban area during air pollution episodes

Linlin Wang[1,2], Junkai Liu[1,5], Zhiqiu Gao[1*], Yubin Li[2], Meng Huang[2], Sihui Fan[2], Xiaoye Zhang[3], Yuanjian Yang[2,6], Shiguang Miao[4], Han Zou[1], Yele Sun[1], Yong Chen[1], Ting Yang[1]

[1]State Key Laboratory of Atmospheric Boundary Layer Physics and Atmospheric Chemistry (LAPC), Institute of Atmospheric Physics, Chinese Academy of Sciences, Beijing 100029, China

[2] Collaborative Innovation Centre on Forecast and Evaluation of Meteorological Disasters, School of Atmospheric Physics, Nanjing University of Information Science and Technology, Nanjing, 210044, China

[3] Chinese Academy of Meteorological Sciences, Beijing, 100081, China

[4] Institute of Urban Meteorology, China Meteorological Administration, Beijing, 100081, China

[5]University of Chinese Academy of Sciences, Beijing 100049, China

[6] State Key Laboratory of Loess and Quaternary Geology, Institute of Earth Environment, Chinese Academy of Sciences, Xi'an 710061, China

Abstract

We investigated the interactions between the air pollutants and the structure of urban boundary layer (UBL) over Beijing by using the data mainly obtained from the 325-m meteorological tower and a Doppler wind lidar during 1–4 December, 2016. Results showed that the pollution episodes in this period could be characterized by low surface pressure, high relative humidity, weak wind, and temperature inversion. Compared with a clean daytime episode that took place on 1 December, results also showed that the attenuation ratio of downward shortwave radiation was about 5%, 24%

*Corresponding author: Dr. Zhiqiu Gao, zgao@mail.iap.ac.cn

and 63% in afternoon hours [from 1200 to 1400 local standard time (LST)] on 2–4 December respectively, while for the net radiation (R_n) attenuation ratio at the 140-m level of the 325-m tower was 3%, 27%, and 68%. The large reduction in R_n on 4 December was not only the result of the aerosols, but also clouds. Based on analysis of the surface energy balance at the 140-m level, we found that the sensible heat flux was remarkably diminished during daytimes on polluted days, and even negative after sunrise (about 0720 LST) till 1400 LST on 4 December. We also found that heat storage in the urban surface layer played an important role in the exchange of the sensible heat flux. Owing to the advantages of the wind lidar having superior spatial and temporal resolution, the vertical velocity variance could capture the evolution of the UBL well. It clearly showed that vertical mixing was negatively related to the concentrating of pollutants, and that vertical mixing would also be weakened by a certain quantity of pollutants, and then in turn worsened the pollution further. Compared to the clean daytime on 1 December, the maximums of the boundary layer height (BLH) reduced about 44% and 56% on 2−3 December, when the average $PM_{2.5}$ (PM_1) concentrations in afternoon hours (from 1200 to 1400 LST) were 44 (48) μg m^{-3} and 150 (120) μg m^{-3}. Part of these reductions of the BLH was also contributed by the effect of the heat storage in the urban canopy.

1 Introduction

In recent years, fine particulate matter (PM) pollution events in the atmospheric boundary layer (ABL), i.e., involving particles with diameters ≤ 2.5 μm ($PM_{2.5}$), have occurred frequently in urban areas, thus emerging as a serious environmental issue in China. The Beijing-Tianjin-Hebei (BTH) metroplex region is one of the most seriously affected areas in China with respect to air pollution. The main hazards or negative effects of air pollution generally fall into two categories: human health and traffic. Thus, it is an issue that has attracted considerable public attention and, accordingly, numerous studies have focused on investigating the sources and formation mechanisms of air pollution in the BTH region, through numerical

simulation and field observational methods (e.g., Wang et al., 2013; Sun et al., 2014; Ye et al., 2016; Li et al., 2017; Han et al., 2018).

Beijing, the main city of the BTH region, has experienced several high-impact, persistent, and severe air pollution episodes in recent years, with notable examples having taken place in January 2013, October and November 2014; December 2015 and 2016, and January 2017. Beijing is located in the North China Plain (NCP), and is surrounded by the Yan and Taihang Mountains from north to west. Therefore, Beijing is frequently affected by thermally induced mountain-plain wind circulation over the NCP, which contributes to the transportation of air pollution in Beijing (Liu et al., 2009; Hu et al., 2014; Chen et al., 2017; Zheng et al., 2018). In addition, it is well recognized that high levels of anthropogenic emissions and rapid formation of secondary aerosol are key factors leading to the frequent occurrence of severe haze episodes (Li et al., 2017). More importantly, these interactions on local and large scales are associated with the meteorological conditions (Sun et al., 2013; Yang et al., 2018). Previous studies have reported that heavy pollution in Beijing is highly related to unfavorable local weather conditions, such as weak wind, strong temperature inversion, high relative humidity (RH) and low surface pressures (Zhang et al., 2014, Liu et al., 2017, Li et al., 2018).

Many studies have also suggested that the structure of the urban boundary layer (UBL), in particular wind, turbulence and stability, had strong influences on the occurrence, maintenance, vertical diffusivity of air pollutants (Han et al., 2009; Zhao et al., 2013). For instance, emissions of air pollution in urban areas lead to a buildup of pollutant concentrations due to reduced mixing and dispersion in UBL (Holmes et al., 2015). An analysis of the dramatic development of a severe air pollution event on November 2014 in the Beijing area revealed that turbulent mixing played an important role in transporting the heavily polluted air and $PM_{2.5}$ oscillations (Li et al., 2018). The vertical profiles of wind and temperature along with the BLH are the main factors affecting turbulence diffusion. Moreover, the BLH is also a key variable in describing the structure of UBL, and in predicting air-pollution (Stull, 1988; Miao et al., 2011; Barlage et al., 2016). Miao et al. (2018) found that the concentration of

$PM_{2.5}$ anti-correlates with the BLH. In addition, air pollutants also can modulate radiative transfer processes through the scattering, reflection and absorption of shortwave radiation and reflection, absorption and emission of longwave radiation (Dickerson et al., 1997; Stone et al., 2008; Wang et al., 2014). In response to reduced solar radiation, the cooling of surface air temperature can lead to strong temperature inversion in the near-surface layer, which can increase the atmospheric stability and prolong the accumulation of pollution because of the existence of this stable boundary layer (Barbaro et al., 2013; Che et al., 2014; Gao et al., 2015). A positive feedback loop in which more aerosol loading leads to a more stable atmospheric boundary layer (ABL), enhanced accumulation of pollutants within the ABL, and a more polluted and hazier atmosphere, was described by Zhang et al. (2013; 2018). It is also found that the further worsened meteorological conditions caused by cumulated aerosol pollution subsequently occurred "explosive growth" of $PM_{2.5}$ mass, which often appears in the late stage of heavy aerosol pollution episode in Beijing-Tianjin-Hebei area in China (Zhong et al., 2017).

Although many studies have provided various interesting findings, consensus has not been reached on the pollutant transport mechanism and the nature of the interactions between the air pollution and the structure of the UBL, mainly due to a lack of reliable and detailed field measurements and the complex properties of the UBL. Additionally, as mentioned above, there are several factors that affect the occurrence of urban air pollution, which can lead to different pollutant transporting mechanism characteristics for different pollution events. Therefore, taking a severe heavy pollution event occurred during 1–4 December, 2016 in Beijing as an example, we will aim to investigate evolution characteristics of ABL structure and further explore the interaction between the structure of the UBL and the air pollution by using the field data collected from a 325-m meteorology tower in Beijing urban area, as well as from a Doppler wind lidar and a dual-wavelength (1064 and 532 nm) depolarization lidar. During this pollution episode, the $PM_{2.5}$ concentration rapidly increased from about 100 μg m^{-3} to approximately 500 μg m^{-3} at 1200 LST on 4 December, which can be considered as a typical case to achieve a better

understanding the formation, transportation, and dispersion mechanisms of the alike pollution event, as well as the interactions between the air pollution and the structure of the UBL.

The paper is organized as follows: Section 2 describes the field site, data, and methods. The overall characteristics of the synoptic pattern and the meteorological factors related to the development of the pollution event are investigated in Section 3. The impacts of the vertical UBL structure evolution on this pollution episode, and vice versa—especially the turbulence due to the radiative forcing of aerosols—are also explored in Section 3. Lastly, the results of the study are summarized in Section 4.

2 Materials

2.1 Site and data

The main data used in this study were from a tall tower in Bejing, officially known as “the Beijing 325-m meteorological tower” which is located at an urban site in the city (39.97°N, 116.37°E; the Beijing “inner-city” site). Within a radius of 5 km of the tower, buildings of different heights are distributed irregularly in all directions, and the area is surrounded by four-story to twenty-story buildings with heights of 10 – 60 m (Liu et al., 2017). The surrounding buildings can be seen in Fig.1a. This tall tower conducts turbulent flux measurements using sonic anemometers (Model Windmaster Pro, Gill, UK) at three different levels (i.e., 47-m, 140-m and 280-m). Note that CSAT3 three-dimensional sonic anemometers designed by Campbell Scientific Inc (USA) at these three levels have been replaced by the Model Windmaster Pro since 2015, so the turbulence measurements before 2015 used in previous papers were collected using the CSAT3 sonic anemometers. The new sonic anemometer experimental setup has been reported by Cheng et al. (2018). Downward-pointing and upward-pointing pyrgeometers and pyranometers (CNR1, Kipp &Zonen) are maintained at the same heights as the sonic anemometers to measure four-component radiation (i.e., incoming shortwave and longwave radiation, and

outgoing shortwave and longwave radiation). Meteorological elements, including wind speed, wind direction (010C cup anemometers and 020C wind vanes, Metone, USA), RH and temperature (HC2-S3, Rotronic, Switzerland) are measured at 15 levels (i.e., 8-m, 15-m, 32-m, 47-m, 65-m, 80-m, 100-m, 120-m, 140-m, 160-m, 180-m, 200-m, 240-m, 280-m and 320-m) above ground level. An Aerodyne aerosol chemical speciation monitor and a high-resolution time-of-flight aerosol mass spectrometer were deployed at 260-m and ground level, repetitively to measure PM_1 mass concentrations at 5-min intervals (Sun et al., 2016).

In addition, wind speed (05103-L, R. M.Young) and temperature (HMP45C, Vaisala) at the 2.2-m level are measured at a surface station about 20 m south of the tower. We also used wind data collected above 100 m by a Doppler wind lidar (Windcube200, Leosphere, Orsay, France) situated on the rooftop of a 8 m high building. Furthermore, a dual-wavelength (1064, and 532 nm) depolarization lidar developed by the National Institute for Environmental Studies, Japan, sits on the rooftop of a 28 m high building (Yang et al., 2017), which provided us with information on aerosols at higher layer. The mass concentrations of $PM_{2.5}$ measured at the Beijing Olympic Sports Center (Aoti surface station) of the National Air Quality Monitoring Network of China using Tapered Element Oscillating Microbalance analyzers with hourly monitored readings, were obtained from the website of China National Environmental Monitoring Center (http://113.108.142.147:20035/emcpublish).

The three-dimensional sonic anemometers original records (10 Hz) were processed, prior to analysis using the methods of double rotation (i.e., yaw and pitch rotations) and linear detrending. Wang et al. (2014) tested a few averaging periods and found that a 1-h averaging period is reasonble at this urban site. The processing of turbulence data in our study followed the method described by Wang et al. (2014).

The criterion of threshold carrier-to-noise ratio (CNR) was used to reduce the effects of invalid data on profiles derived from the Doppler velocities. The data control process was described in detail by Huang et al. (2017). We calculated the vertical velocity variance and stream wise wind speed and wind direction over a

30-minute segment.

The dual-wavelength depolarization lidar was used to retrieve the aerosol vertical structure at a spatially resolved resolution of 6 m and temporally resolved resolution of 10 s, but only for altitudes in excess of 100 m because of an incomplete overlap between the telescopic field of view and the laser beam. For this study the raw temporal resolution of the retrieved aerosol profiles was set at 30-minute. More details on the lidar instruments and various data processing techniques were provided by (Yang et al., 2017).

The NCEP FNL (Final) Operational Global Analysis data collected every six hours, at 0200, 0800, 1400 and 2000 LST, on 1°×1° grids were used to analyze the synoptic-scale weather conditions.

2.2 Methods

2.2.1 Turbulent flux and radiation calculation

The sensible heat and latent heat fluxes were calculated using the eddy-covariance method:

$$H = \rho C_p \overline{w'T'} \quad (1)$$

$$LE = L_v \overline{w'q'} \quad (2)$$

where ρ is the air density (kg m^{-3}), C_P is the specific heat capacity at constant pressure (J kg^{-1} K^{-1}), w is the vertical velocities (m s^{-1}) from the sonic anemometers, T is the air temperature (K), L_v is the the latent heat of vaporization of water (J kg^{-1}), and q is the specific humidity (kg kg^{-1}). The overbar denotes time averages and an averaging period of 60 minutes was used in this study.

The surface energy budget (SEB) without consideration of horizontal advection is usually formulated as

$$R_n + Q_F = H + LE + G \quad (3)$$

where H is the sensible heat flux from the surface to the adjacent air, LE is the latent heat flux into the atmosphere associated with evapotranspiration, and G is the ground and urban canopy heat storage. R_n is the net radiation, which can be described as

$$R_n = DSR - USR + DLR - ULR \quad (4)$$

DSR stands for downward shortwave radiation, USR for upwelling short-wave radiation, DLR for downward incoming long-wave radiation, and ULR for upwelling long-wave radiation. The anthropogenic heat flux (Q_F)is a significant term in urban areas, which is the additional energy released by human activities, however its estimation is difficult due to the absence of accurate energy consumption and traffic flow data. In this study, heat storage term minus the anthropogenic heat flux, $G - Q_F = R_n - H - LE$, will be analyzed

2.2.2 Determination of UBL depths

Lidar techniques have become one of the most valuable and popular systems to detect the atmosphere because of their higher spatiotemporal resolution. As a result, many techniques have been developed to determine the BLH by using the remote sensing instruments, such as radar wind profilers, aerosol lidars, and ground-based microwave radiometers (Flamant et al., 1997; Emeis et al., 2004, Haman et al., 2012). Remote sensing is particularly useful in analyzing vertical profiles of turbulence mixing in UBL, and is generally easier to deploy than radiosondes (Georgoulias et al., 2009).

Recently, the turbulence method to define the BLH has been proposed by using the Doppler lidar which can obtain three-dimensional wind. The vertical velocity variance σ_w^2 can be used to describe the density of the turbulence, hence the height of the layer in which vertical velocity variance σ_w^2 exceeds a given threshold is considered as the BLH. Previous investigators have given different values of σ_w^2 for different underlying surfaces (Tucker et al., 2009, Pearson et al. 2010). Barlow et al. (2011) defined the mixing height as the height over London, UK up to which σ_w^2 >

225 0.1 $m^2 s^{-2}$. Here, we select this method of Barlow et al. (2011), because of the similar
226 urban fraction between central Beijing and London.

227 The 30-min vertical velocity standard deviation between lidar is

228 $$\sigma_w = \sqrt{\frac{1}{N-1}\sum_{i=1}^{N}(w_i - \bar{w})^2} \quad (5)$$

229 Where N is the record number every 30 minutes, w_i denotes the *i*th vertical velocity
230 (m s^{-1}), and $\bar{w}$ is the mean vertical wind speed.

231 3 Results and discussion

232 3.1 Air pollution episodes in Beijing

233 As shown in Fig. 1c, the visibility around the 325-m tower at about 1400 LST on
234 3 December was much lower than that on 1 December. In fact, the visibility decreased
235 rapidly from 1200 to 1600 LST before sunset (1650 LST) on 3 December,
236 accompanied by the increasing $PM_{2.5}$ concentration (from 100 μg m^{-3} to 200 μg m^{-3})
237 at the Olympic Sports Center station and PM_1 concentration (from 100 μg m^{-3} to 190
238 μg m^{-3}) at the 325-m tower station (Fig. 2). After sunset, the $PM_{2.5}$ hourly maximum
239 concentration reached 530 μg m^{-3} at 0200 LST 4 December. The cumulative
240 explosive growth process of the pollution, starting at 1200 3 December and lasting till
241 0200 LST 4 December, is defined as cumulative stage (CS).

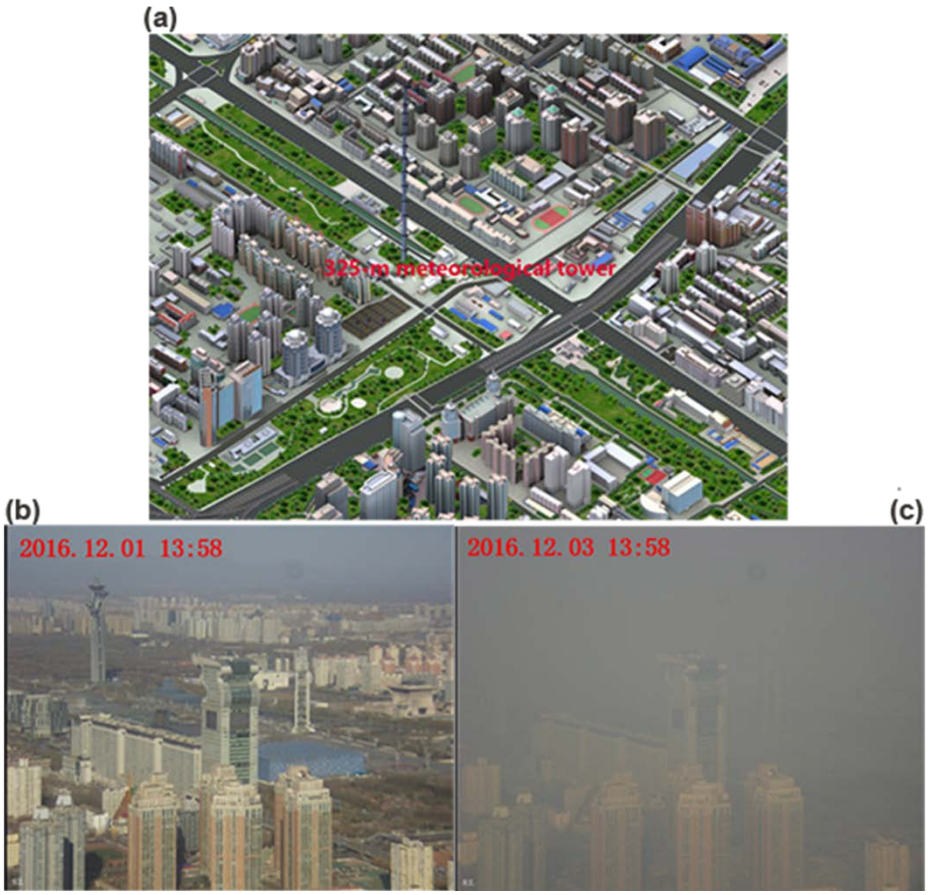

Figure 1: (a) Three-dimensional graph of the underlying surface around the 325-m tower in Beijing. Photographs of the buildings looking north from the 280-m level of the 325-m tower at 1358 LST (b) 1 December and (c) 3 December, 2016.

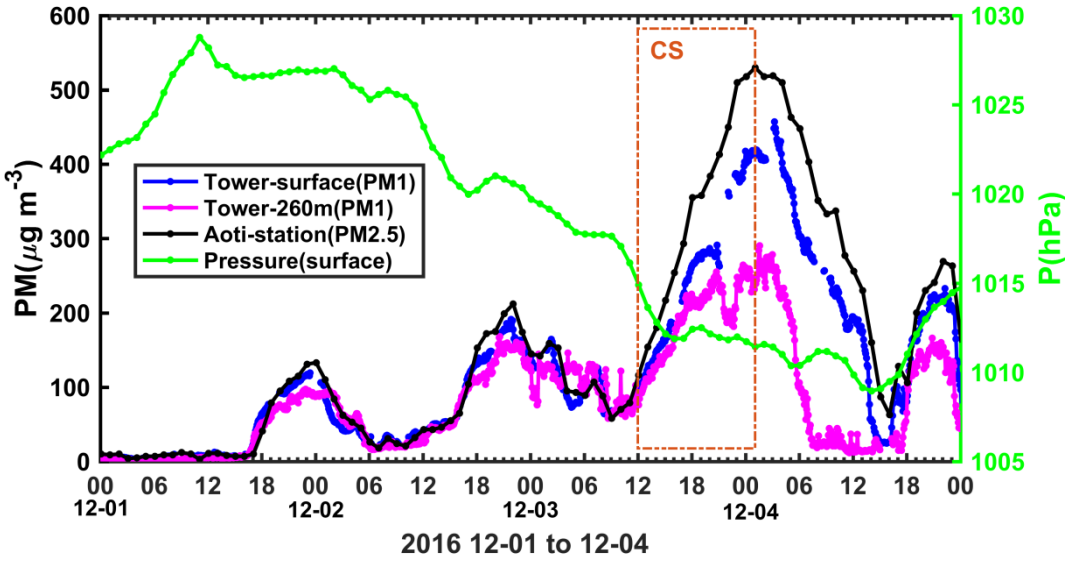

Figure 2: Temporal variation of the PM_1 observed at the surface and the 260-m level of the 325-m tower, $PM_{2.5}$ at Aoti surface station, and surface pressure at the surface station of the IAP, during 1–4 December 2016. (red box: CS)

The surface pressure measured at the Institute of Atmospheric Physics (IAP)

surface station (Fig. 2) indicated the air quality was getting worse with decreasing surface pressure. In order to analyze the synoptic background fields for the CS, the sea level pressure and surface wind field on 3 December are shown in Fig. 3. At 0800 LST, the Beijing region was governed by a saddle type pressure field characterized by uniform pressure, very weak wind speed and changeable wind direction. The surface high pressure system over the Bohai and Yellow seas was conducive to the maintenance of these stagnant meteorological conditions till 1400 LST, which provided the unfavorable meteorological conditions for the diffusion of air pollutants and contributed to the formation of CS.

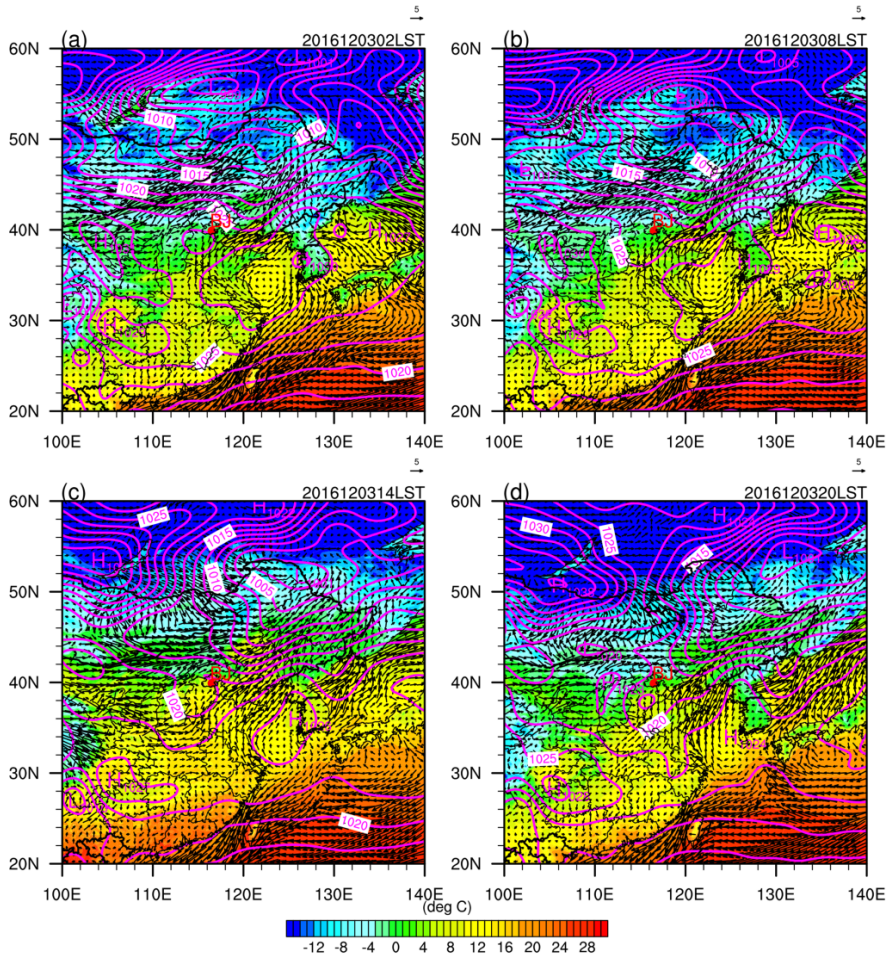

Figure 3: Distribution of surface pressure and temperature at (a) 0200 LST, (b) 0800 LST, (c) 1400 LST, and (d) 2000 LST 3 December 2016, where the green star marks the location of Beijing (BJ).

3.2 Meteorological parameters

As shown in Fig. 4a, RH was mostly larger than 40% during pollution episodes,

and increasing along with the concentrated $PM_{2.5}$ (PM_1). Especially during the CS, RH could reach near to 100% at nighttime, which firstly appeared at the levels of 160–220 m and then extended to the lower levels. Meanwhile, the deeper RH (>80%) with higher PM concentrations during the CS was possibly caused by secondary aerosol formation. Due to aerosol cooling force, θ at the daytime on 3 December was much lower than on other days. Clearly, the wind flow played an important role in the air pollution process. The Southwesterly wind transported air pollutants from Hebei Province to Beijing on the first two pollution nights (Fig. 4c). In order to investigate the characteristics of the UBL structure, the vertical gradients of potential temperature ($\Delta\theta = \theta_2 - \theta_1$) and gradient absolute values in wind speed ($|\Delta U| = |U_2 - U_1|$) were calculated by using the adjacent two levels as the thermal and dynamic factors (Fig. 5). It was found that the vertical gradients of wind speed and potential temperature were small because of strong vertical thermal mixing during daytime, whereas they were large at nighttime due to weak vertical mixing. Temperature inversions were found at all three nights, which was negative to the dispersion of the pollutants (Li et al., 2018; Wang et al., 2019). Typically, the formation of temperature inversions in winter night is associated with the radiative cooling effect. Zhong et al. (2019) found that the temperature reduction because of the aerosol cooling force during daytime induced or reinforced an inversion, and then this enhanced inversions further worsen the aerosol pollution. This two way feedback mechanism between unfavorable meteorological conditions and cumulative aerosol pollution also appeared in our case. The values of $\Delta\theta$ and the duration of $\Delta\theta > 0$ increased day by day, meaning the thermal stability strengthened with worsening polluted days. Moreover, a long-term existence of temperature inversion near the surface could be found till 1200 LST 4 December, associated with extremely steady stability. This stable surface stratification resulted in the suppressed diffusion of air pollutants at the surface, causing a dissipation lag for PM_1 at the surface compared to the case at the 260-m level (shown in Fig. 2).

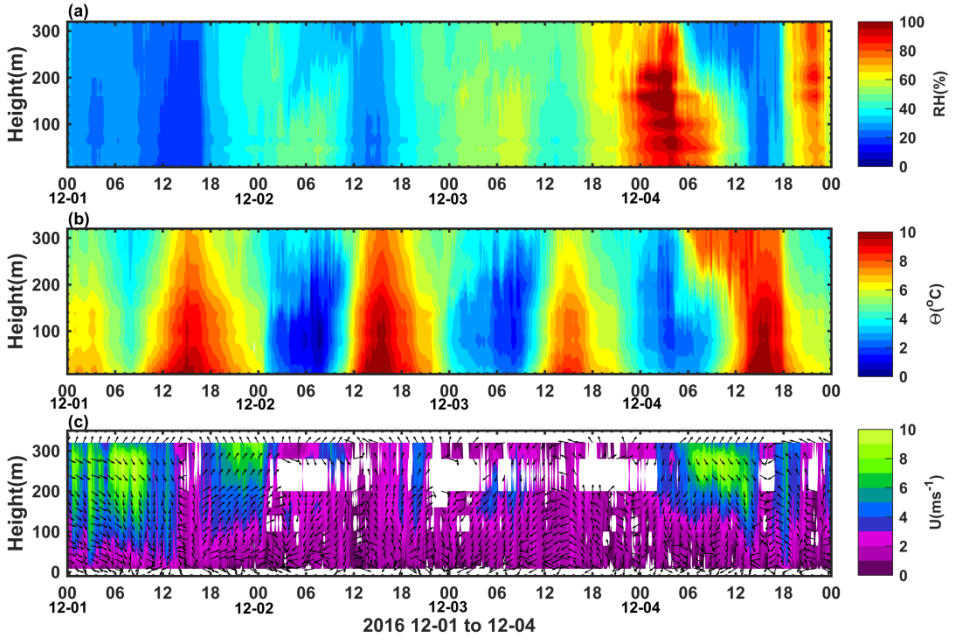

Figure 4: Vertical evolution of (a) relative humidity, (b) virtual temperature, and (c) wind speed and wind vectors (arrows), observed at 15 levels of the 325-m tower during 1–4 December 2016.

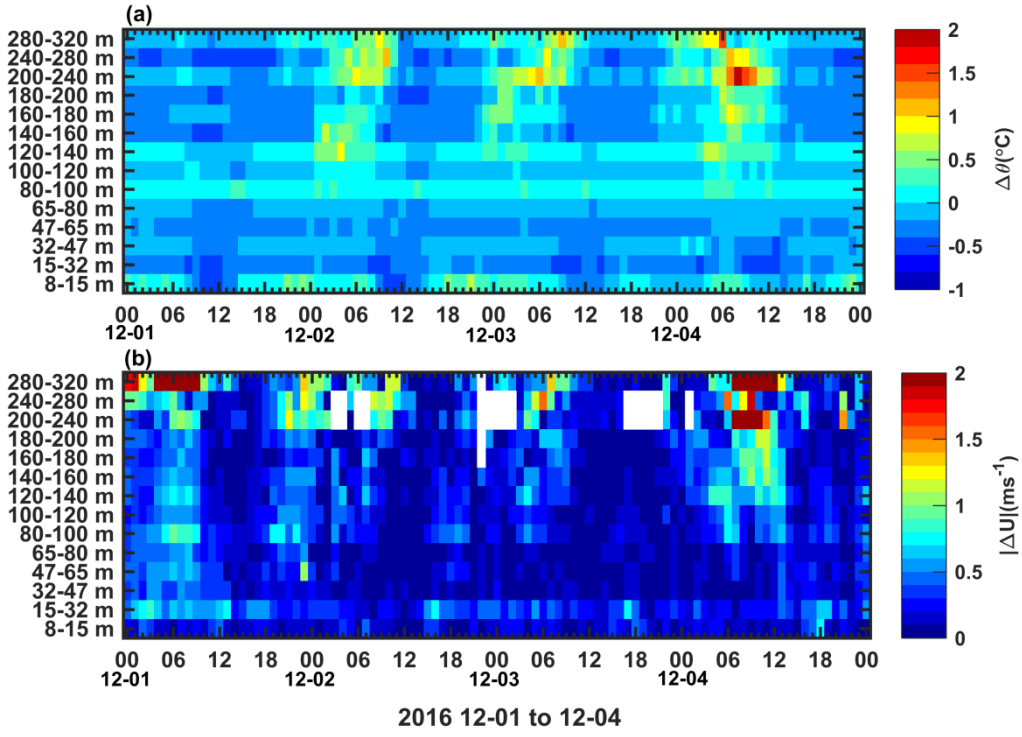

Figure 5: Vertical evolution of (a) vertical gradients of relative potential temperature and (b) vertical gradients of zonal wind speed, based on observations at 15 levels of the 325-m tower during 1–4 December 2016.

Owning to the limited height of the tower, the wind profile above several

hundred meters collected by the Dopper lidar (Fig. 6) can be used to further investigate the association between the wind flow and air pollution process. On 1 December, the air quality was good before noon and there was strong northwest wind (mostly around 10 m s^{-1}) at 200–1000 m levels above the ground (ATG). In our case, notably, a low-level jet (LLJ) established after sunset, with the jet core at 300–500 m ATG, and the maximum wind speed was around 10 m s^{-1} at about 2400 LST. We can see the $PM_{2.5}/PM_1$ concentration was starting to increase after sunset with the maximum $PM_{2.5}$ concentration (120 μg m^{-3}) observed at 2400 LST, and then decreased with the gradually weakened LLJ, which suggests this southwesterly LLJ transferred polluted air from the south by advection to Beijing before midnight. A previous study also reported that presence of an LLJ can increase the surface pollution through horizontal advection (Hu et al., 2013). Besides the horizontal advection, LLJ also can generate vertical mixing due to the wind shear with large $|\Delta U|$ (> 1 ms^{-1}). Once the northern maintain flow generated, the LLJ became weaker (< 5 ms^{-1}) in the early morning on 2 December, and then the vertical mixing generated by the weakened LLJ changed to the dominated term which made an important contribution to the mixing of the pollutants at the dissipated period. Chen et al. (2018) also pointed out that a northerly weak LLJ noticeably reduced the PM concentration in urban Beijing. As a result, the presence of an LLJ has an indispensable effect on the process of the air pollution in the nocturnal boundary layer (NBL).

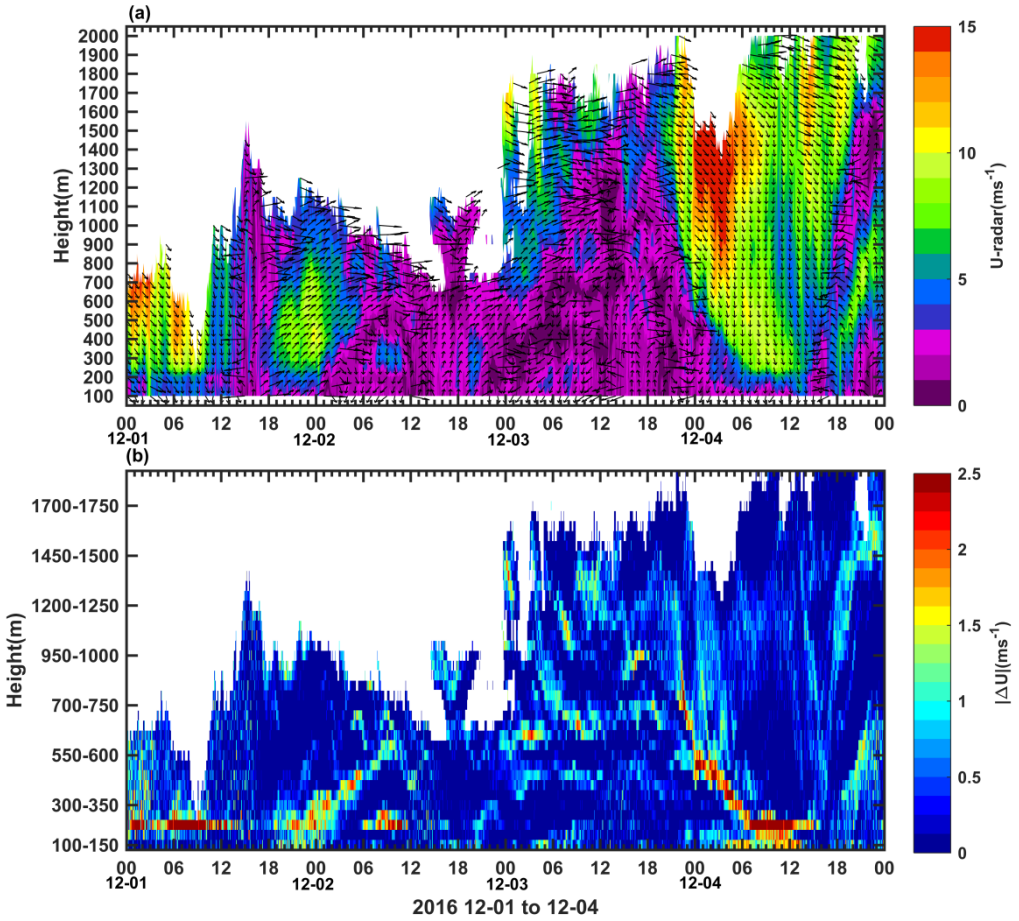

Figure 6: Vertical evolution of (a) wind speed and (b) vertical gradients of wind speed, based on Doppler wind lidar observations during 1–4 December 2016.

We can also see that the PM_1 concentration at the 260-m level started to decrease at 0200 LST 2 December which was about two hours later than PM_1 at the ground level. This could be explained that the gradually deep and clean northwest mountain-plain wind occurred first below 100 m ATG, and then reached the upper level. On 2 December, the wind below 1 km was dominated by speeds of around 2 m s^{-1} from 0600 to 2200 LST. The weak northerly winds did not fully disperse the air pollutants before the noon. Meanwhile, after the transition time on 1300 LST, southerly winds existed and brought polluted air from the south, and then the air quality became worsened, and the maximum $PM_{2.5}$ concentration (210 μg m^{-3}) occurred at 2200 LST. Compared to early morning on 2 December, the wind below 600 m was weaker and the vertical gradients (Fig. 6b) were much smaller, meaning mechanical turbulence (vertical mixing) was extremely weak. Thus, there is no

dramatic reduction in the air pollution before sunrise on 3 December, and then the CS began at noon when the wind speeds were mostly lower than 3 m s^{-1} below 1 km ATG, because of the saddle–type pressure-field background (Fig. 3).

3.3 SEB characteristics

Solar radiation is the most important driver of the development of the UBL. Various climatic changes within urban ABL are driven by the SEB, which distributes the energy by radiation, convection and conduction between a facet (Oke et al., 2017). Therefore, the SEB, described as Eq. 3, is a fundamental aspect contributing to our understanding of the variations in the UBL.

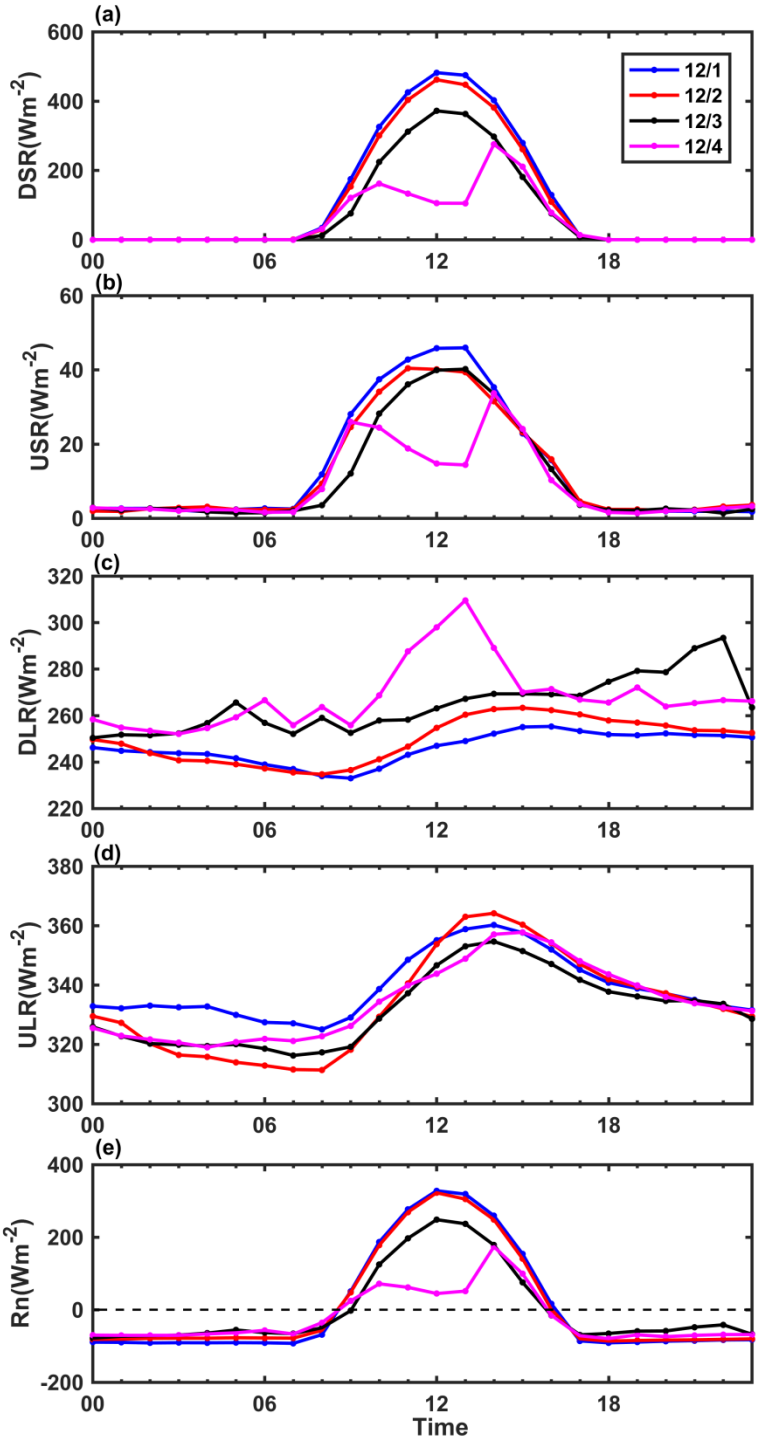

Figure 7: Diurnal cycle of (a) downward shortwave radiation, (b) upward shortwave radiation, (c) downward longwave radiation, (d) upward longwave radiation, and (e) net radiation, observed at the 140-m level of the 325-m tower during 1–4 December 2016.

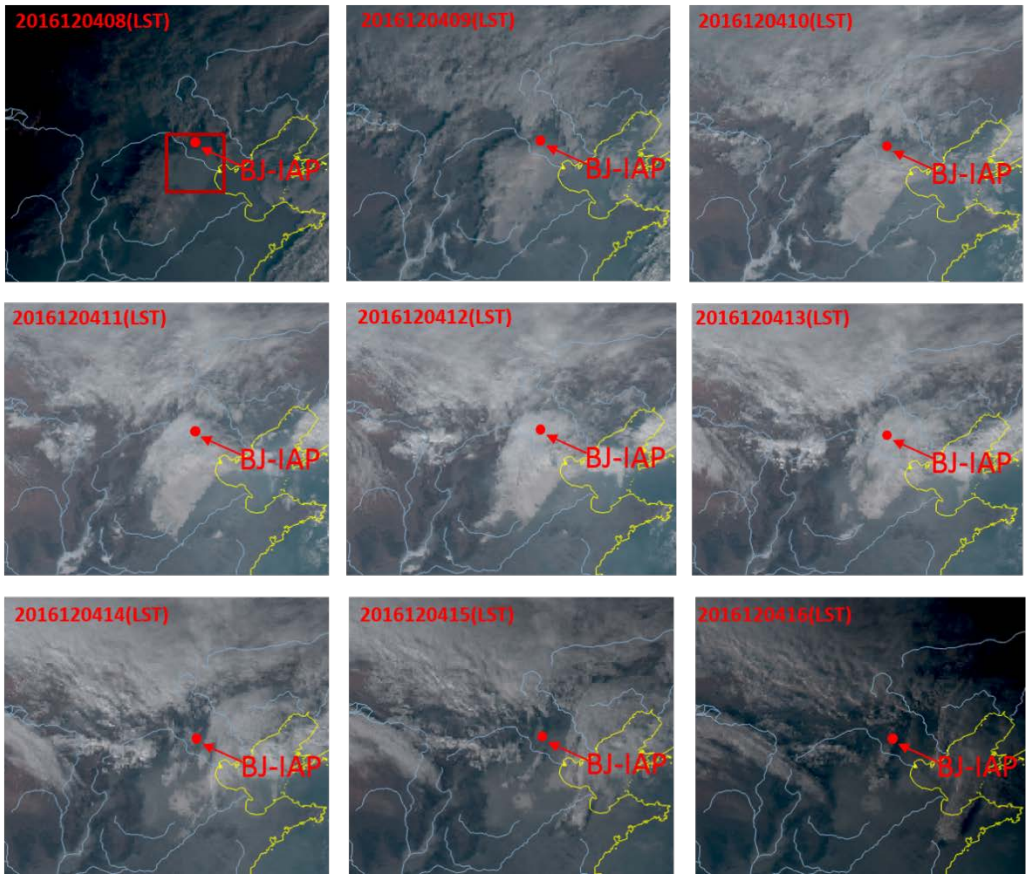

Figure 8: Hourly Himawari-8 geostationary meteorological satellite cloud images from 0800 LST to 1600 LST 4 December, where the red point marked the location of IAP station in Beijing, and the red square marked the mass of grey.

In this study, we wanted to focus on the SEB at one level rather than the vertical difference at between different levels. Moreover, measurements at the 140-m are above the roughness sublayer layer and are within the surface layer (Miao et al. 2012), hence only the observations at the 140-m level were used in studying the radiative exchange. In Fig. 7, the four components shows the daytime pollution received less shortwave radiation but more longwave radiation than the daytime clean episode. The *DSR* reduces with gradually worsening air quality on a day-to-day basis. The *DSR* during this 4-day period reached a peak value (482 W m^{-2}) at 1200 LST 1 December. The differences between the daytime clean and pollution episodes reached about 20 and 110 W m^{-2} at 1200 LST on 2 and 3 December. On 4 December, the largest difference was 376 W m^{-2} at 1200 LST, followed by 1400 LST (127 W m^{-2}), which approximates that at 1400 LST on 3 December (105 W m^{-2}). Overall, compared with the *DSR* during the daytime clean episode on 1 December, the attenuation ratio of the

DSR was about 4%, 23% and 78% at 1200 LST 3–4 December, and the averaged value was 5%, 24% and 63% afternoon hours (1200–1400 LST), respectively. Many efforts have been made on the radiative forcing due to the increasing aerosols loading by using model simulations and field experiments (Ramanathan et al., 2001; Xia et al. 2007; Ding et al., 2016). Based on observations at the 140-m level at 325-m tower under eight cloudless days (three clean days and five pollution days) in January 2015, Wang et al. (2016) found that the maximum attenuation of the *DSR* was 33.7 W m^{-2} and the attenuation ratio was 7.4% at 1200 LST. Due to the difference in solar angle, degree of pollution, pollutant component, cloud etc., attenuation differences are expected in different case studies. Here, the *USR* on clean days was larger than in pollution days with a larger maximum difference (32 W m^{-2}) on 4 December, which was mainly caused by the lower quantity of *DSR* received on 4 December. For the *DLR*, the diurnal change in the difference between 1 December and 2 December was insignificant. During the other two daytimes, the *DLR* increased with the enhancement of pollution level, and the peak values on 3 December and 4 December were respectively 51 W m^{-2} and 56 W m^{-2}.

The diurnal variation of the *DSR* on December 4 was discontinuous, which suggests the large attenuation of the *DSR* on this day was not only the impact of the higher aerosol concentrations, but also that of the cloud cover. The largest *DLR* on 4 December also indicated the possibility existence of clouds. Information on the coverage of clouds can be seen from satellite cloud images, which in this case were provided by the products of the Himawari-8 geostationary meteorological satellite, launched by the Japan Meteorological Agency (http://www.eorc.jaxa.jp/ptree/). According to these data, the first three days were free from clouds (figures are omitted). From the mass of grey marked by the red square in Fig. 8, it is apparent that pollutants dominated the BTH region at 0800 LST, and then this area became partially cloudy. The area over Beijing was covered with cloud at 1000 LST, which lasted about 3 hours, and then at 1500 LST had become cloudless. Van de Heever and Cotton (2007) found giant nuclei could lead to strong early enhancement of cloud development. Moreover, previous studies have found that cloud fraction changes with

aerosol loading (Gunthe et al., 2011; Che et al., 2016). In our case, before the cloudy day, heavy pollutants occurred over the BTH region, and the IAP station recorded high relative humidity (> 90%, shown in Fig. 4) at midnight, which would have enhanced aerosol hygroscopic growth, implying significant aerosol–cloud interactions, referred to Che et al. (2016). Thus, we can deduce that the cloud cover over the BTH region may in part account for the aerosols on the pollution days, which supports the abundant cloud condensation nuclei (CNN) for the cloud formation on the following day. Certainly, further studies with more measurements data and model simulations are needed to validate this conclusion.

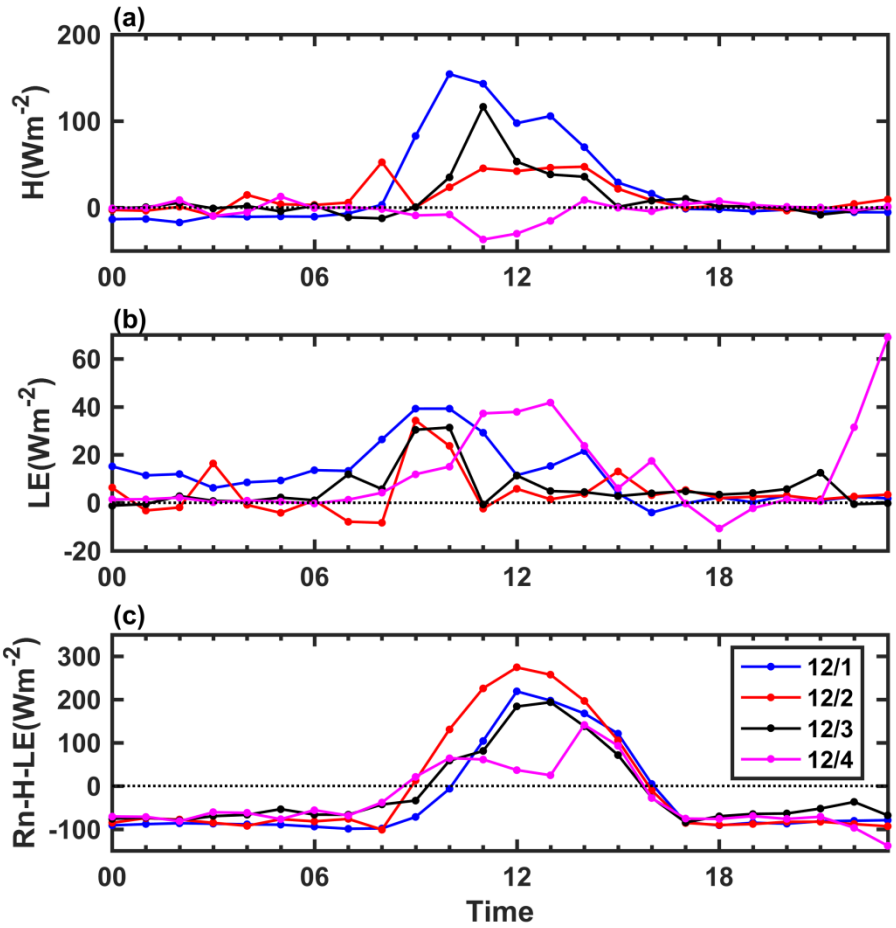

Figure 9: Diurnal cycle of (a) sensible heat flux, (b) latent heat flux, and (c) heat storage minus anthropogenic heat (termed as $R_n - H -$ LE), observed at the 140-m level of the 325-m tower during 1–4 December 2016.

In general, the R_n (shown in Fig. 7) attenuation ratio was 3%, 27%, and 68% respectively, in the afternoon hours, 2–4 December. This attenuation of the radiation

414 in pollution days directly resulted in the change of the SEB. In Fig. 9, clearly, *LE* was
415 extremely low, at less than 50 W m^{-2} during this 4-day period in winter. The peak
416 value of the *H* was about 154 W m^{-2}, 53 W m^{-2}, and 117 W m^{-2}, on 1–3 December,
417 respectively. On 3 December, the heat flux showed a dramatically decrease, e.g. from
418 117 W m^{-2} to 53 W m^{-2} in one hour (1100−1200 LST), which aggravated the negative
419 effect on pollutants diffusion (corresponding to the CS). There was a thick
420 temperature inversion near to the surface that lasted till the afternoon on 4 December,
421 as described in last section, which resulted in the downward heat transfer (H<0) to the
422 urban surface in daytime. Gao et al. (2015) also found that large positive radiative
423 forcing reduced the *H* and *LE* by 5–16 W m^{-2} and 1–5 W m^{-2} during a severe fog–
424 haze event over the NCP, by using WRF-Chem model simulations. By analyzing the
425 measurements collected at a rural site (farmland) Gucheng in Hebei Province from 1
426 December 2016 to 31 January 2017 in winter, Liu et al. (2018) confirmed that the
427 mean daily maximum *H* was only 40 W m^{-2} on heavily polluted days (daily mean
428 $PM_{2.5}$ concentration > 150 μg m^{-3}), but reached 90 W m^{-2} on clean days (daily mean
429 $PM_{2.5}$ concentration < 75 μg m^{-3}). Model simulations have pointed out that the
430 reduced sensible heat resulting from aerosol backscattering could lower the air
431 temperature and suppress the growth of the ABL (Yu et al. 2002). In our case, the
432 large reductions of *H* on 2–4 December also imply that the high $PM_{2.5}$ (PM_1)
433 concentrations from the nighttime till after sunrise may have
434 suppressed on the evolution of the UBL. Further and more detailed investigation into
435 the development of the UBL was reported in the next section.

436 Mostly, during daytime, $G - Q_F$ was the largest consuming term in the SEB,
437 accounting for about 65 %, 83 %, 78 % and 71 % averaged in the afternoon hours
438 (1200–1400 LST) on 1–4 December, respectively. Although changes in Q_F at IAP
439 site are unknown due to unavailable accurate energy consumption and traffic flow
440 data, the Q_F term, an additional energy source, is always positive and can be
441 assumed similarly during different days in a short term. Thus, the larger ratio of
442 $G - Q_F$ relative to R_n ($(G - Q_F)/R_n$) implies much more heat is stored in the urban

canopy, compared with other terms. Heat storage can be affected by different factors including atmospheric conditions (e.g., solar radiation, air temperature and wind speed) and urban characteristics (e.g., urban morphology, material properties and layout configuration) (Meehl and Tebaldi 2004; Lindberg and Grimmond 2011; Miralles et al., 2014; Sun et al., 2017). Urbanization results in land-cover change from vegetative to urban surfaces, and modifies the fractional coverage of urban. The fraction of impervious surfaces around the 325-m tower was investigated using an analytical footprint model and found to exceed 65% (Wang et al., 2015). Such large fraction of impervious urban surfaces in Beijing leads to large urban heat capacity. During the early morning on 2 December, the air temperature near the surface (illustrated in Fig. 4) was lower than on other mornings (i.e., at around 0400 LST, about 5°C lower than on 1 December at 2-m level ABG) and dropped to around zero, meaning a large amount of heat was lost from the urban volume. Then after sunrise, due to the high thermal conductivity of the concrete (about 65 times as large as the air), a considerable part of the R_n (maximum reaching 85% at 1200 LST for $G - Q_F$) was balanced by the heat storage in the urban fabric. Compared with 1 December, the larger heat storage with similar R_n (differing by less than 16 W m^{-2}) on 2 December led to weaker heat flux, which was negative to the diffusion of the pollutants, with a slight increasing tend from 0900 LST to noon, (illustrated in Fig. 2). Specifically, under the conditions of early morning, much more solar heat is absorbed to warm the large urban fabric after sunrise. Besides, previous studies have demonstrated wind was a key determinant of changes in storage heat and the increasing amount of daytime heat storage in urban canopy was strongly tied to lower wind speeds (Grimmomd and Oke, 1999; Vautard et al., 2010; Sun et al., 2017). Thus, in this case, the weaker wind (Fig. 4c), associated with weak turbulent transport, contributed the larger heat storage ratios during polluted daytime, in particular on 2 December. Compared with the rural surface, Kotthaus and Grimmond (2014) reported the heat storage in urban surfaces led to delayed warming/cooling after sunrise/sunset, which resulted in the nocturnal stable conditions generally developing later (Barlow et al., 2015). In our study, generally, over the urban surface, compared with the clean

daytime, the polluted daytime with calm wind condition not only had reduced R_n and but also larger heat storage ratio, which would result in weaker heat flux.

To improve our understanding of the role of the SEB in air pollution process, more work is needed, such as consideration of the uncertainty in eddy-covariance observations over complex heterogeneous urban surfaces and Q_F. Q_F is a very important term of SEB in urban areas (Sailor 2011, Chow et al., 2014), and this additional heat release will enhance H then increases the air temperature and BLH (Yu et al., 2014). Yang et al. (2018) found that incorporating anthropogenic heat emissions into the modeling system was effective in improving air quality predictions in Beijing. More specific studies in the impacts of the Q_F on the meteorology and air quality of the Greater Beijing area can be made by urban-rural contrast with more observational data, or numerical models in further study.

3.4 Development of the UBL

The diurnal cycle of the ABL exerts strong control on the scalar concentrations of air pollutants (Oke et al., 2017). It is known that the ABL starts to grow after sunrise, and deepens to a maximum value in mid-afternoon, then decreases with the falling off solar radiation reaching at ground surface, during which the whole layer is convectively unstable and well mixed and is defined as CBL. After sunset, accompanied by diminishing turbulence, the boundary-layer depth declines rapidly, and then the boundary layer becomes to the NBL. Based on the general changes in BLH, the TKE at a certain depth or the amount of solar radiation, previous studies have proven that vertical mixing affects pollutants diffusion (Guinot et al., 2006; Sun et al., 2013; Guo et al., 2017). However, few have documented the diurnal circle of the intensity variation of vertical mixing in the UBL, on account of the limitation of instruments. Here, we took advantages of the Dopper lidar (superior spatial and temporal resolution), to quantify the values of the vertical mixing, described as vertical velocity variance σ_w^2 on clean and polluted days.

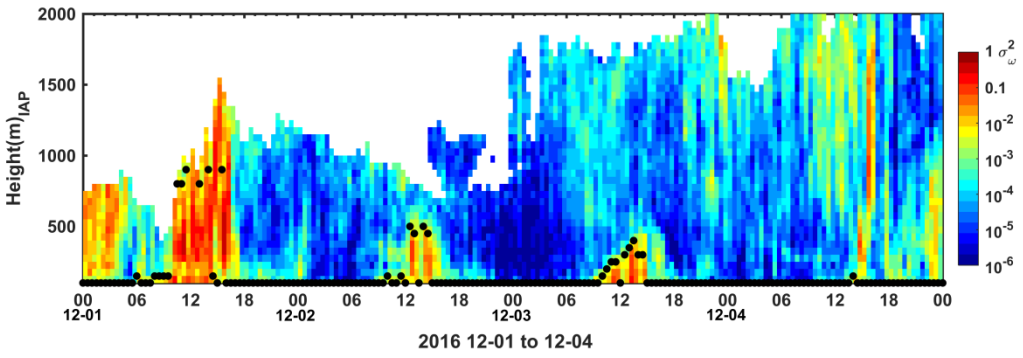

Figure 10: Velocity variance, σ_w^2 (m^2 s^{-2}), calculated from the Doppler wind lidar data. Derived planetary boundary layer depths, based on the threshold method, are depicted as black dots.

As presented in Fig. 10, it was found that the variance of σ_w^2 could characterize the development of the UBL. σ_w^2 became greater after sunrise (0720 LST), then reached a maximum at about 1400 LST, exhibiting an obvious trend of decline (from σ_w^2>10^{-1} to σ_w^2<10^{-2} $m\,s^{-1}$) after sunset (1650 LST). When the UBL developed into NBL, σ_w^2 was about 10^{-3} $m\,s^{-1}$ at the 200−300 m levels till midnight and decreased to about 10^{-4} $m\,s^{-1}$ after midnight until sunset. σ_w^2 was obviously lower and its vertical distribution shallower during daytime pollution episodes compared with the daytime clean episode, which is consistent with the results concluded by analysis of SEB. The diminished R_n and enhanced heat storage ratio during polluted daytime on 2-4 Dec resulted in the weak vertical mixing. On 4 December, the vertical mixing was extremely weak, ranging from 10^{-4} to 10^{-5}, and there was barely any diurnal variation of σ_w^2 till 1500 LST when the $PM_{2.5}$ (PM_1) had completely dissipated, which suggests the radiative cooling of aerosols and cloud was a major factor of influence in the UBL development by suppressing vertical mixing. Weak turbulence in this stagnating UBL could not broke the deep temperature inversion (Fig. 5a), and such shallow UBL seemed to act an umbrella, blocking the entrainment with cold-clean air at the upper level, and solar radiation to the surface, and in return, further suppressing the diffusion of pollutants, leading to not only the increasing $PM_{2.5}$ (PM_1) concentration during the CS but also much slower diffusion of PM_1 at the surface than that at the 260-m level (Fig. 2). Accordingly, in our case study, the

two-way feedback mechanism between air pollutants and the UBL is strikingly responsible for the cumulative and dissipation stage of these pollution episodes.

Compared to 1 December, the vertical mixing was weaker till about 5 hours after the sunrise on 2 December (CS). This weak evolution of the CBL was consistent with the weak sensible heat flux (Fig. 9). As discussed in Section 3.3, a large amount of the heat was trapped in the cold urban fabrics under calm wind condition (Fig. 2), resulting in poor sensible heat flux after sunrise and weak vertical mixing on 2 December.

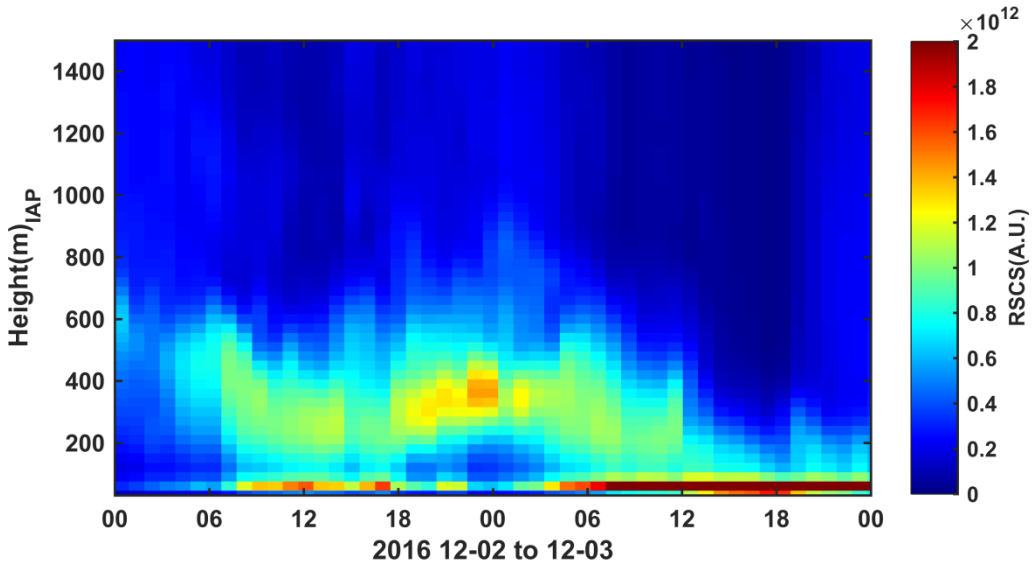

Figure 11: Evolution of the lidar range-squared-corrected signal (RSCS) at 532 nm from 1200 LST 2 December to 1200 LST 3 December 2016. The color scale indicates the intensity of the RSCS, and warm colors represent stronger light scattering.

Additionally, the σ_w^2 was mainly ranged from10^{-6} to 10^{-5} m s^{-1} ATG to the detectable observing height during the nighttime from 2200 LST 2 December till the early morning 0500 LST before the CS on 3 December. This ultra-weak turbulence transport maintained a very shallow and stable NBL. Note that values of the PM_1 concentration (Fig. 2) at the 260-m height of the 325-m tower changed slightly with the time during the ultra-weak turbulence transport periods. Moreover, before the CS on 3 December, the aerosol lidar data (Fig. 11) showed that the gradient of the range-squared-corrected signals (RSCS, calculated by $(RS\text{-}RS_0)r^2$, is applied to compensate for range-related attenuation from the atmosphere, where the lidar signal *RS* is corrected for the background noise contribution due to atmospheric

546 skylight and electronic noise of the instrumentation used, the RS_0 is the background
547 signal, and r is the range between the lase source and the target) between the levels of
548 200–250 m and 400–500 m ATG were larger than the other levels from 1800 LST
549 (after sunset) 2 December to 0500 LST (before sunrise) 3 December. As we know,
550 both aerosols and water vapor affect the signals of the lidar. The larger RSCS at the
551 time mentioned above, in our case, must not only have been because of the water
552 vapor but also aerosol concentrations, being consistent with the larger PM_1
553 concentration at the 260-m level (more than 100 μg m^{-3}). Similarly, the larger RSCS
554 between the levels of 200–250 m and 400–500 m ATG illustrated these levels were
555 accumulated with high levels of pollutants and the vertical distribution of pollutants
556 was inhomogeneous, all of which implies that the 260-m level may have been in the
557 residual layer. The pollutants in the residual layer are known to play an important role
558 in the diurnal changes of pollutants at the surface (Hastie et al., 1993; Berkowtiz et al.,
559 2000; Salmond and Mckendary, 2006). Sun et al. (2013) suggested that the high
560 concentration of particles in the residual layer could reach the ground the following
561 morning through convection, causing severe pollutant concentrations in Beijing. In
562 the Tianjin area, Han et al. (2018) also found that a pollution layer was present at the
563 altitude of 1000 m in the early morning on 16 December, 2016, where the aerosols in
564 the higher layers were transmitted to the ground by downward flow before the
565 formation of heavy pollution. Actually, many studies have focused on this mechanism
566 of pollutant vertical mixing in a stable NBL from the micrometeorology perspective.
567 Turbulence in a very stable NBL is typically intermittent and generated by mechanical
568 shear associated with changes in wind velocity with height (Mahrt et al., 1998),
569 referred to as upside-down turbulence in an upside-down boundary structure,
570 compared to the convective daytime case (Mahrt, 1999; Mahrt and Vickers, 2002).
571 This upside-down structure is characterized by TKE (or σ_w^2) and turbulent fluxes
572 increasing with height, and negative transportation of TKE or velocity variances
573 (Banta et al., 2006). As shown in Fig. 10, the σ_w^2 became larger at lower levels from
574 0500 LST 3 December, and then the largest values of σ_w^2 existed at the 500–600 m,
575 along with the corresponding $|\Delta U|$ shown in Fig. 6b. This turbulence could transport

the pollutants accumulated in the residual layer downward to the lower levels, and contributed to the later CS of the pollution. Halios and Barlow (2018) also suggested that shear production dominates in the upper half of the UBL, and could therefore not be neglected, even in cases with low wind. Consequently, the intermittent turbulence generated by the wind shear above a sable UBL plays an important role in the vertical spreading of pollutants.

As a key variable describing the structure of the UBL, the urban BLH estimated using the threshold method ($\sigma_w^2 > 0.1$ m^2 s^{-2}) from the Doppler lidar data is also shown in Fig. 10. For the CBL, the diurnal variations of CBL height were not described well by the threshold method for these 4-day, and especially on 4 December for the weak turbulence on polluted day. Eventually, this empirical method was derived using data in autumn or summer, during which the vertical turbulence is much greater than in the winter. In our study, the criterion $\sigma_w^2 > 0.1$ m^2 s^{-2} was not applicable because of weak vertical turbulence transport ($\sigma_w^2 < 0.1$ m^2 s^{-2}) at certain times of the day. The threshold method was also invalid in the NBL during this study period. This may be because of the weak vertical turbulence or smaller height of the NBL falling below the observable height (100 m). Using Windcube100 data during summer in Beijing, Huang et al. (2017) also pointed that this method was reasonable for estimating the CBL depth, while it failed to determine the planetary boundary layer depths for late-night. Subsequently, they defined the NBL top as the height at which the vertical velocity variance decreases to 10 % of its near-surface maximum minus a background variance. However, this new method for the depth of the NBL also failed in our studied period (figure omitted). This is because the NBL in winter is mostly steady, which does not satisfy the near-neutral assumption for the method developed by Huang et al. (2017). Additionally, the NBL has been a major problem for meteorologists for a long time, especially over polluted urban canopies, which make the problem far more complex. Therefore, further investigation of this method should be made in future.

Miao et al. (2018) pointed out that the BLH of a fully developed CBL was clearly anti-correlated with the daily $PM_{2.5}$ concentration, implying that the change in

606 the BLH in the afternoon plays an important role in pollution levels, which is similar
607 with our present. Furthermore, the mixing heights of the fully coupled CBL for 1–4
608 December were about 900 m, 500 m, and 400 m, respectively. Due to the weaker
609 mixing intensity on 4 December, it is difficult to capture specific values of the BLH.
610 As shown in Fig. 2, the maximum daily $PM_{2.5}$ (PM_1) concentrations increased
611 day-by-day from 1 to 3 December, indicating high pollutants concentration near the
612 surface coincide with a shallow CBL. Petäjä et al. (2016) reported that aerosol–
613 boundary layer feedback remained moderate at fine PM concentrations lower than
614 200 μg m^{-3} in Nanjing area, but became intensive at higher PM loadings, and the
615 BLH reduced to half of the original height at particle mass concentrations slightly
616 above 200 μg m^{-3}. Similarly, particularly strong interactions were verified in the
617 Beijing area when the $PM_{2.5}$ mass concentration was larger than 150–200 ug m^{-3}
618 (Luan et al., 2018). In our investigation, the BLH was reduced by about 44% on 2
619 December with the low $PM_{2.5}$ (PM_1) concentration 46 (48) μg m^{-3} and only a 5%
620 attenuation of *Rn*. Additionally, for the $PM_{2.5}$ (PM_1) concentration of 180 (150) μg m^{-3}
621 on 3 December, a 56% reduction of the BLH was found with a 27% attenuation of R_n.
622 Therefore, in addition to the R_n term, it is important to note that the heat storage term
623 in the SEB also makes a significant contribution to the reduction of BLH (details
624 discussed in Section 3.3). Especially, over the megacity Beijing with large fraction of
625 impervious surface, heat storage accounts a great mount of net radiation and its ratio
626 increases with decreasing wind speed, which should be excluded from the quantitative
627 analysis of the impact of aerosol pollutants on UBL. Otherwise, the response degree
628 of the UBL to aerosol pollutants would be overestimated, owing to the polluted days
629 mostly accompanied with weak wind in Beijing.

630 Note that, the BLH reduced significantly from 1 December to 2 December, while
631 the $PM_{2.5}/PM_1$ concentration increased only a little, which implied that the reduced
632 BLH must be a negative factor, yet not the only one, to the dispersion of pollutants.
633 As mentioned in the introduction part, heavy pollution in Beijing is also highly related
634 to high relative humidity (RH), which is positive to the rapid formation of secondary
635 aerosol. On 3 December, during the period, after sunrise before the CS, with weak

winds, appreciable near-surface moisture accumulation appeared with RH over 60% (Fig. 4 c, a), while the RH was about 40% after sunrise on 2 December. Based on the previous studies (Tie et al., 2017; Zhong et al., 2019), such enhanced moisture on 3 December would reduce direct radiation through accelerating liquid-phase and heterogeneous reactions to produce more secondary aerosols and enhancing aerosol hygroscopic growth to increase aerosol particle size and mass (Kuang et al., 2016), which would back-scatter more solar radiation to space. Thus, the lower RH on 2 December was negative to the formation of secondary aerosol, resulting in the less $PM_{2.5}/PM_1$ on 2 December concentration than on 3 December. Moreover, the sustained stagnant condition on 2 December contributed to a certain degree of the $PM_{2.5}/PM_1$ concentration before CS, which was one of the preconditions for the rapid formation of CS.

In general, the main impacts of synoptic conditions (pressure, wind, temperature, relative humidity, etc.), surface energy balance on the UBL evolution, and then the interactions between the aerosol pollutants and UBL structure can be highly summarized by a schematic diagram in the present study (Fig. 12), providing a critical reference for air pollution forecast and assessment in Beijing.

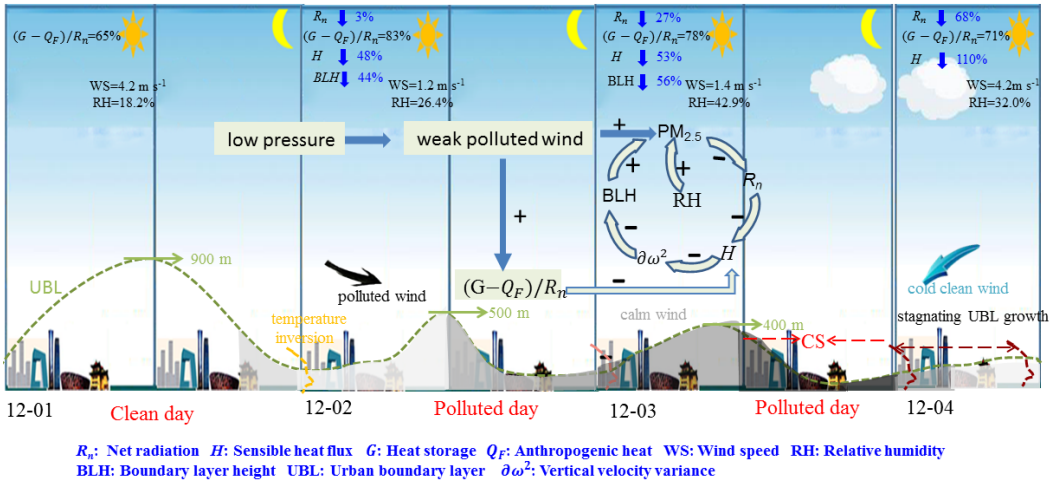

R_n: Net radiation H: Sensible heat flux G: Heat storage Q_F: Anthropogenic heat WS: Wind speed RH: Relative humidity
BLH: Boundary layer height UBL: Urban boundary layer $\partial\omega^2$: Vertical velocity variance

Figure 12: Schematic diagrams of the roles of synoptic conditions, surface energy budget in the development of UBL, and the two-way feedback between UBL structure and accumulation of $PM_{2.5}$ during 1–4 December 2016, the values of meteorological elements averaged in noon hours (1200–1400 LST).

4 Conclusion

Using data from the 325-m meteorological tower in Beijing and two nearby

660 lidars, we investigated the characteristics of UBL structure during 1–4 December,
661 2016 in Beijing and examined the interaction between the structure of the UBL and
662 the air pollution during three pollution episodes, especially the rapid CS during which
663 the $PM_{2.5}$ concentration rose from about 100 μg m^{-3} to 500 μg m^{-3} in 12 hours. The
664 main conclusions can be summarized as follows.

665 1) During this 4-day study period, the air pollution gradually worsened on a
666 day-by-day basis, with deceasing surface air pressure. Specially, the large-scale
667 circulation with a saddled pressure field was highly unfavorable for the dispersion of
668 pollutants on 3 December during the CS. The RH was larger than 40% during the
669 heavy pollution episodes, and the vertical distribution of RH showed a remarkably
670 inhomogeneous pattern during the peak period of the CS with the deep RH (> 80%) at
671 the 47–240-m levels and heavy surface $PM_{2.5}/PM_1$ concentration (about 500 μg
672 m^{-3}/400 μg m^{-3}) in the early morning on 4 December. Temperature inversion ($\Delta\theta > 0$)
673 occurred during all three nights. For the first pollution episode during the nighttime on
674 1-2 December, a southern neutral LLJ was found at the 200–1000-m levels after
675 sunset till midnight over Beijing, which transported the pollutants from the south of
676 Beijing by advection. For the second episode during nighttime on 2–3 December,
677 weak southerly wind (<3 m s^{-1}) dominated below 600-m level, with small vertical
678 gradients, due to the saddle–type pressure-field background. Meanwhile, for CS on 3
679 December, there was a very deep and weak wind layer, which extended to about
680 1100-m level till 2200 LST 3 December, when the accumulated $PM_{2.5}$ concentration
681 was larger than 400 μg m^{-3} at the surface.

682 2) Compared with the *DSR* during the daytime clean episode on 1 December, the
683 attenuation ratio of the DSR was about 5%, 24% and 63%, respectively, in the
684 afternoon hours (1200–1400 LST) 2–4 December, which mainly caused a 3%, 27%
685 and 68% reduction of the $R_{n.}$ The large attenuation of solar radiation on 4 December
686 resulted from the cloud caused by the large aerosol loading with high RH on 3
687 December, possibly supporting plentiful CNN for the formation of cloud. Generally,
688 the latent heat exchange term was very low during these four days over the urban
689 canopy in Beijing, and the dominate term was mostly the heat storage minus

anthropogenic heat, calculated as $R_n - H - LE$, during daytime, which accounted for about 65%, 83%, 78% and 71% of R_n (averaged 1200–1400 LST) on 1–4 December, respectively. We also found that the lower *H* appeared on the polluted days than on the clean days, which partly caused by the large consuming term of the heat storage in the urban fabric with calm wind condition.

3) In the CBL, the diurnal circle of lidar-based σ_w^2 agreed with the variation of the diurnal cycle of *H* estimated by the eddy-covariance method at the 140-m level of the 325-m tower, showing that vertical mixing was obviously weakened on polluted days. Compared to the clean day, the evolution of the UBL was delayed by about 5 hours after sunrise (about 0720 LST) on 4 December, because of the long-term (> 12 hours) existence of temperature inversion resulting from the effects of both aerosols and clouds. This stagnating UBL seemed to act like an umbrella, suppressing the diffusion of PM_1 at the surface, which was cleaned at about 1500 LST, while the PM_1 at the 260-m level was driven away by the strong clean northerly wind flow at about 0700 LST. Therefore, this two-way feedback mechanism between air pollutants and the UBL was strikingly responsible for the cumulative and dissipation stage of this pollution event in our case. Additionally, the intermittent turbulence generated by the wind shear above the stable NBL in the early morning on 3 December may have contributed to the CS through the downward transporting pollutants from the residual layer. Compared to 1 December the reduction of the maximum BLH was 44% on 2 December and 56% on 3 December, whereas, the BLH on 4 December was unobtainable due to the stagnating UBL growth.

Acknowledgements

This work was funded by the National Key Research and Development Program of the Ministry of Science and Technology of China (2016YFC0203304 and 2017YFC0209601) and the open funding of State Key Laboratory of Loess and Quaternary Geology (SKLLQG1842).

References

Banta, R. M., Pichugina, Y. L., and Brewer, W. A.: Turbulent velocity-variance

719 profiles in the stable boundary layer generated by a nocturnal low-level Jet, J. Atmos.
720 Sci., 63, 2700-2719, 10.1175/JAS3776.1, 2006.
721 Barbaro, E., Vilà-Guerau de Arellano, J., Krol, M. C., and Holtslag, A. A. M.: Impacts
722 of aerosol shortwave radiation absorption on the dynamics of an idealized convective
723 atmospheric boundary layer, Boundary-Layer Meteorol., 148, 31-49,
724 10.1007/s10546-013-9800-7, 2013.
725 Barlage, M., Miao, S. G., and Chen, F.: Impact of physics parameterizations on
726 high-resolution weather prediction over two Chinese megacities, J. Geophys. Res.,
727 121, 10.1002/, 2016.
728 Barlow, J. F., Halios, C. H., Lane, S. E., and Wood, C. R.: Observations of urban
729 boundary layer structure during a strong urban heat island event, Environ. Fluid
730 Mech., 15, 373-398, 10.1007/s10652-014-9335-6, 2014.
731 Berkowitz, C. M., Fast, J. D., and Easter, R. C.: Boundary layer vertical exchange
732 processes and the mass budget of ozone: Observations and model results, J. Geophys.
733 Res., 105, 14789-14805, 10.1029/2000jd900026, 2000.
734 Bowen, B. M., Baars, J. A., and Stone, G. L.: Nocturnal wind direction shear and its
735 potential impact on pollutant transport, J. Appl. Meteorol., 39, 437-445,
736 10.1175/1520-0450(2000)039<0437:NWDSAI>2.0.CO;2, 2000.
737 Che, H. C., Zhang, X. Y., Wang, Y. Q., Zhang, L., Shen, X. J., Zhang, Y. M., Ma, Q. L.,
738 Sun, J. Y., Zhang, Y. W., and Wang, T. T.: Characterization and parameterization of
739 aerosol cloud condensation nuclei activation under different pollution conditions, Sci.
740 Rep., 6, 24497, 10.1038/srep24497, 2016.
741 Che, H., Xia, X., Zhu, J., Li, Z., Dubovik, O., Holben, B., Goloub, P., Chen, H.,
742 Estelles, V., Cuevas-Agulló, E., Blarel, L., Wang, H., Zhao, H., Zhang, X., Wang, Y.,
743 Sun, J., Tao, R., Zhang, X., and Shi, G.: Column aerosol optical properties and aerosol
744 radiative forcing during a serious haze-fog month over North China Plain in 2013
745 based on ground-based sunphotometer measurements, Atmos. Chem. Phys., 14,
746 2125-2138, 10.5194/acp-14-2125-2014, 2014.
747 Chen, Y., An, J. L., Sun, Y. L., Wang, X. Q., Qu, Y., Zhang, J. W., Wang, Z. F., and
748 Duan, J.: Nocturnal low-level winds and their impacts on particulate matter over the
749 Beijing area, Adv. Atmos. Sci., 35, 1455-1468, 10.1007/s00376-018-8022-9, 2018.
750 Chen, Y., An, J. L., Wang, X. Q., Sun, Y. L., Wang, Z. F., and Duan, J.: Observation of
751 wind shear during evening transition and an estimation of submicron aerosol
752 concentrations in Beijing using a Doppler wind lidar, J. Meteor. Res., 31, 350-362,
753 10.1007/s13351-017-6036-3, 2017.
754 Cheng, X. L., Liu, X. M., Liu, Y. J., and Hu, F.: Characteristics of CO_2 concentration
755 and flux in the Beijing urban area, J. Geophys. Res., 10.1002/2017jd027409, 2018.
756 Chow W.T. L., Salamanca F. P., Georgescu M., Mahalov A., Milne J. M. and Ruddell
757 B. L.: Amulti-method and multi-scale approach for estimating city-wide
758 anthropogenic heat fluxes, Atmos. Environ. 99, 64–76,
759 10.1016/j.atmosenv.2014.09.053,2014.
760 Dickerson, R. R.: The Impact of Aerosols on Solar Ultraviolet Radiation and
761 Photochemical Smog, Science, 278, 827-830, 10.1126/science.278.5339.827, 1997.
762 Ding, A. J., Huang, X., Nie, W., Sun, J. N., Kerminen, V. M., Petäjä, T., Su, H., Cheng,
763 Y. F., Yang, X. Q., Wang, M. H., Chi, X. G., Wang, J. P., Virkkula, A., Guo, W. D.,
764 Yuan, J., Wang, S. Y., Zhang, R. J., Wu, Y. F., Song, Y., Zhu, T., Zilitinkevich, S.,
765 Kulmala, M., and Fu, C. B.: Enhanced haze pollution by black carbon in megacities in
766 China, Geophys. Res. Lett., 43, 2873-2879, 10.1002/2016gl067745, 2016.
767 Emeis, S., Münkel, C., Vogt, S., Müller, W. J., and Schäfer, K.: Atmospheric
768 boundary-layer structure from simultaneous SODAR, RASS, and ceilometer

769 measurements, Atmos. Environ., 38, 273-286, 10.1016/j.atmosenv.2003.09.054, 2004.
770 Farrugia, R. N.: The wind shear exponent in a Mediterranean island climate,
771 Renewable Energy, 28, 647, 10.1016/S0960-1481(02)00066-6, 2003.
772 Flamant, C., Pelon, J., Flamant, P. H., and Durand, P.: Lidar determination of the
773 entrainment zone thickness at the top of the unstable marine atmospheric boundary
774 layer, Boundary-Layer Meteorol., 83, 247-284, 1997.
775 Gao, Y., Zhang, M., Liu, Z., Wang, L., Wang, P., Xia, X., Tao, M., and Zhu, L.:
776 Modeling the feedback between aerosol and meteorological variables in the
777 atmospheric boundary layer during a severe fog–haze event over the North China
778 Plain, Atmos. Chem. Phys., 15, 4279-4295, 10.5194/acp-15-4279-2015, 2015.
779 Georgoulias, A. K., Papanastasiou, D. K., Melas, D., Amiridis, V., and Alexandri, G.:
780 Statistical analysis of boundary layer heights in a suburban environment, Meteorol.
781 Atmos. Phys., 104, 103-111, 10.1007/s00703-009-0021-z, 2009.
782 Grimmond C. S. B. and Oke T. R.: Aerodynamic properties of urban areas derived,
783 from analysis of surface form, J. Appl. Meteorol., 38 1262–92, 10.1175/1520-0450,
784 1999.
785 Guinot, B., Roger, J. C., Cachier, H., Wang, P. C., Bai, J. H., and Yu, T.: Impact of
786 vertical atmospheric structure on Beijing aerosol distribution, Atmos. Environ., 40,
787 5167-5180, 10.1016/j.atmosenv.2006.03.051, 2006.
788 Gunthe, S. S., Rose, D., Su, H., Garland, R. M., Achtert, P., Nowak, A., Wiedensohler,
789 A., Kuwata, M., Takegawa, N., Kondo, Y., Hu, M., Shao, M., Zhu, T., Andreae, M. O.,
790 and Pöschl, U.: Cloud condensation nuclei (CCN) from fresh and aged air pollution in
791 the megacity region of Beijing, Atmos. Chem. Phys., 11, 11023-11039,
792 10.5194/acp-11-11023-2011, 2011.
793 Guo, J. P., Xia, F., Zhang, Y., Liu, H., Li, J., Lou, M. Y., He, J., Yan, Y., Wang, F., Min,
794 M., and Zhai, P. M.: Impact of diurnal variability and meteorological factors on the
795 $PM_{2.5}$ - AOD relationship: Implications for $PM_{2.5}$ remote sensing, Environ. Pollut.,
796 221, 94-104, 10.1016/j.envpol.2016.11.043, 2017.
797 Halios, C. H., and Barlow, J. F.: Observations of the morning development of the
798 urban boundary layer over London, UK, taken during the ACTUAL project,
799 Boundary-Layer Meteorol., 166, 395-422, 10.1007/s10546-017-0300-z, 2018.
800 Haman, C. L., Lefer, B., and Morris, G. A.: Seasonal variability in the diurnal
801 evolution of the boundary layer in a near-coastal urban environment, J. Atmos. Ocean.
802 Technol., 29, 697-710, 10.1175/jtech-d-11-00114.1, 2012.
803 Han, S. Q., Bian, H., Tie, X. X., Xie, Y. Y., Sun, M. L., and Liu, A. X.: Impact of
804 nocturnal planetary boundary layer on urban air pollutants: measurements from a
805 250-m tower over Tianjin, China, J. Hazard Mater., 162, 264-269,
806 10.1016/j.jhazmat.2008.05.056, 2009.
807 Han, S. Q., Hao, T. Y., Zhang, Y. F., Liu, J. L., Li, P. Y., Cai, Z. Y., Zhang, M., Wang,
808 Q. L., and Zhang, H.: Vertical observation and analysis on rapid formation and
809 evolutionary mechanisms of a prolonged haze episode over central-eastern China, Sci.
810 Total Environ., 616-617, 135-146, 10.1016/j.scitotenv.2017.10.278, 2018.
811 Hastie, D. R., Shepson, P. B., Sharma, S., and Schiff, H. I.: The influence of the
812 nocturnal boundary layer on secondary trace species in the atmosphere at Dorset,
813 Ontario, Atmos. Environ., 27A, 533-541, 10.1016/0960-1686(93)90210-P, 1993.
814 Holmes, H. A., Sriramasamudram, J. K., Pardyjak, E. R., and Whiteman, C. D.:
815 Turbulent fluxes and pollutant mixing during wintertime air pollution episodes in
816 complex terrain, Environ. Sci. Technol., 49, 13206-13214, 10.1021/acs.est.5b02616,
817 2015.
818 Hu, X. M., Klein, P. M., Xue, M., Zhang, F. Q., Doughty, D. C., Forkel, R., Joseph, E.,

819 and Fuentes, J. D.: Impact of the vertical mixing induced by low-level jets on
820 boundary layer ozone concentration, Atmos. Environ., 70, 123-130,
821 10.1016/j.atmosenv.2012.12.046, 2013.
822 Hu, X. M., Ma, Z. Q., Lin, W. L., Zhang, H. L., Hu, J. L., Wang, Y., Xu, X. B.,
823 Fuentes, J. D., and Xue, M.: Impact of the Loess Plateau on the atmospheric boundary
824 layer structure and air quality in the North China Plain: a case study, Sci. Total
825 Environ., 499, 228-237, 10.1016/j.scitotenv.2014.08.053, 2014.
826 Huang, M., Gao, Z. Q., Miao, S. G., Chen, F., LeMone, M. A., Li, J., Hu, F., and
827 Wang, L. L.: Estimate of boundary-layer depth over Beijing, China, using Doppler
828 Lidar data during SURF-2015, Boundary-Layer Meteorol., 162, 503-522,
829 10.1007/s10546-016-0205-2, 2017.
830 Kotthaus, S., and Grimmond, C. S. B.: Energy exchange in a dense urban
831 environment – Part I: Temporal variability of long-term observations in central
832 London, Urban Clim., 10, 261-280, 10.1016/j.uclim.2013.10.002, 2014.
833 Kuang, Y., Zhao, C.S., Tao, J.C., Bian, Y.X., Ma, N., Impact of aerosol hygroscopic
834 growth on the direct aerosol radiative effect in summer on North China Plain, Atmos.
835 Environ., 147(2016), pp. 224-233, 10.1016/j.atmosenv.2016.10.013, 2016.
836 Lee, X. H., Gao, Z. Q., Zhang, C. L., Chen, F., Hu, Y. Q., Jiang, W. M., Liu, S. H., Lu,
837 L. H., Sun, J. L., Wang, J. M., Zeng, Z. H., Zhang, Q., Zhao, M., and Zhou, M. Y.:
838 Priorities for boundary layer meteorology research in China, Bull. Am. Meteorol. Soc.,
839 96, ES149-ES151, 10.1175/bams-d-14-00278.1, 2015.
840 Li, J., Sun, J. L., Zhou, M. Y., Cheng, Z. G., Li, Q. C., Cao, X. Y., and Zhang, J. J.:
841 Observational analyses of dramatic developments of a severe air pollution event in the
842 Beijing area, Atmos. Chem. Phys., 18, 3919-3935, 10.5194/acp-18-3919-2018, 2018.
843 Li, X., Zhang, Q., Zhang, Y., Zhang, L., Wang, Y. X., Zhang, Q. Q., Li, M., Zheng, Y.
844 X., Geng, G. N., Wallington, T. J., Han, W. J., Shen, W., and He, K. B.: Attribution of
845 $PM_{2.5}$ exposure in Beijing–Tianjin–Hebei region to emissions: implication to control
846 strategies, Sci. Bull., 62, 957-964, 10.1016/j.scib.2017.06.005, 2017.
847 Li, Z. Q., Guo, J. P., Ding, A. J., Liao, H., Liu, J. J., Sun, Y. L., Wang, T. J., Xue, H.
848 W., Zhang, H. S., and Zhu, B.: Aerosol and boundary-layer interactions and impact on
849 air quality, Natl. Sci. Rev., 4, 810-833, doi:https://doi.org/10.1093/nsr/nwx117, 2017.
850 Lindberg F. and Grimmond C. S. B.: The influence of vegetation and building
851 morphology on shadow patterns and mean radiant temperatures in urban areas: model
852 development and evaluation, Theor. Appl. Climatol. 105, 311–323,
853 10.1007/s00704-010-0382-8, 2011.
854 Liu, C. W., Gao, Z. Q., Li, Y. B., Gao, C. Y., Su, Z. B., and Zhang, X. Y.: Surface
855 energy budget observed at a winter wheat field site in the north China plain during a
856 fog-haze event, Boundary-Layer Meteorol., 10.1007/s10546-08-0407, 2018.
857 Liu, J. K., Gao, Z. Q., Wang, L. L., Li, Y. B., and Gao, C. Y.: The impact of
858 urbanization on wind speed and surface aerodynamic characteristics in Beijing during
859 1991–2011, Meteorol. Atmos. Phys., 130, 311-324, 10.1007/s00703-017-0519-8,
860 2017.
861 Liu, S. H., Liu, Z. X., Li, J., Wang, Y. C., Ma, Y. J., Sheng, L., Liu, H. P., Liang, F. M.,
862 Xin, G. J., and Wang, J. H.: Numerical simulation for the coupling effect of local
863 atmospheric circulations over the area of Beijing, Tianjin and Hebei Province, Sci.
864 China Ser. D, 52, 382-392, 10.1007/s11430-009-0030-2, 2009.
865 Luan, T., Guo, X. L., Guo, L. J., and Zhang, T. H.: Quantifying the relationship
866 between $PM_{2.5}$ concentration, visibility and planetary boundary layer height for
867 long-lasting haze and fog-haze mixed events in Beijing, Atmos. Chem. Phys., 18,
868 203-225, 10.5194/acp-18-203-2018, 2018.

Mahrt, L., and Vickers, D.: Contrasting vertical structures of nocturnal boundarylayers, Boundary-Layer Meteorol., 105, 351-363, 10.1023/A:1019964720989, 2002.
Mahrt, L., Sun, J. l., Blumen, W., Delany, T., and Oncley, S.: Nocturnal boundary-layer regimes, Boundary-Layer Meteorol., 88, 255-278, 10.1023/A:1001171313493, 1998.
Mahrt, L.: Stratified atmospheric boundary layers, Boundary-Layer Meteorol., 90, 375–396, 1999.
Meehl G. A. and Tebaldi C.: More intense, more frequent, and longer lasting heat waves in the 21st century, Science, 305 994–997, 10.1126/science.1098704, 2004.
Miao, S. G., Chen, F., Li, Q. C., and Fan, S. Y.: Impacts of urban processes and urbanization on summer precipitation: A case study of heavy rainfall in Beijing on 1 August 2006, J. Appl. Meteorol. Climatol., 50, 806-825, 10.1175/2010jamc2513.1, 2011.
Miao, S. G., Dou, J. X., Chen, F., Li, J., and Li, A. G.: Analysis of observations on the urban surface energy balance in Beijing. Sci. China Earth Sci., 55(11), 1881-1890, 10.1007/s11430=012-4411-6, 2012.
Miao, Y. C., Guo, J. P., Liu, S. H., Zhao, C., Li, X. L., Zhang, G., Wei, W., Ma, Y. J.: Impacts of synoptic condition and planetary boundary layer structure on the trans-boundary aerosol transport from Beijing-Tianjin-Hebei region to northeast China. Atmos. Environ. 181, 1-11, 10.1016/j.atmosenv.2018.03.005, 2018.
Miralles D.G., Teuling A. J., van Heerwaarden C. C. and de Arellano J .V-G.: Mega-heatwave temperatures due to combined soil desiccation and atmospheric heat accumulation, Nat. Geosci., 7, 345–349, 10.1038/NGEO2141, 2014.
Oke, T. R., Mills, G., Christen, A., and Voogt, J. A.: Urban climates, Cambridge University Press, Cambridge, 157pp, 2017.
Pearson, G., Davies, F., and Collier, C.: Remote sensing of the tropical rain forest boundary layer using pulsed Doppler lidar, Atmos. Chem. Phys., 10, 5891-5901, 2010.
Petäjä, T., Järvi, L., Kerminen, V. M., Ding, A. J., Sun, J. N., Nie, W., Kujansuu, J., Virkkula, A., Yang, X. Q., Fu, C. B., Zilitinkevich, S., and Kulmala, M.: Enhanced air pollution via aerosol-boundary layer feedback in China, Sci. Rep., 6, 18998, https://doi.org/10.1038/srep18998, 2016.
Ramanathan, V., Crutzen, P. J., Kiehl, J. T., and Rosenfeld, D.: Aerosols, climate, and the hydrological cycle, Science, 294, 2119-2126, 10.1126/science.1064034, 2001.
Sailor D. J.: A review ofmethods for estimating anthropogenic heat and moisture emissions in the urban environment Int. J. Climatol. 31, 189–99, 10.1002/joc.2106, 2011.
Salmond, J. A., and McKendry, I. G.: A review of turbulence in the very stable nocturnal boundary layer and its implications for air quality, Prog. Phys. Geog., 29, 171-188, 10.1191/0309133305pp442ra, 2005.
Stone, R. S., Anderson, G. P., Shettle, E. P., Andrews, E., Loukachine, K., Dutton, E. G., Schaaf, C., and Roman, M. O.: Radiative impact of boreal smoke in the Arctic: Observed and modeled, J. Geophys. Res., 113, 10.1029/2007jd009657, 2008.
Stull, R. B.: An Introduction to Boundary Layer Meteorology, Atmospheric Sciences Library, 8, 89 pp., 1988.
Sun, T., Kotthaus, S., Li, D., Ward, H.C., Gao, Z., Ni, G.-H., Grimmond, C.S.B.: Attribution and mitigation of heat wave-induced urban heat storage change. Environ. Res. Lett. 12, 114007, 10.1088/1748-9326/aa922a, 2017.
Sun, Y. L., Jiang, Q., Wang, Z. F., Fu, P. Q., Li, J., Yang, T., and Yin, Y.: Investigation of the sources and evolution processes of severe haze pollution in Beijing in January

2013, Journal of Geophysical Research: Atmospheres, 119, 4380-4398, 10.1002/, 2014.
Sun, Y. L., Wang, Z. F., Wild, O., Xu, W. Q., Chen, C., Fu, P. Q., Du, W., Zhou, L. B., Zhang, Q., Han, T. T., Wang, Q. Q., Pan, X. L., Zheng, H. T., Li, J., Guo, X. F., Liu, J. G., and Worsnop, D. R.: "APEC Blue": Secondary aerosol reductions from emission controls in Beijing, Sci. Rep., 6, 20668, 10.1038/srep20668, 2016.
Sun, Y., Song, T., Tang, G. Q., and Wang, Y. S.: The vertical distribution of $PM_{2.5}$ and boundary-layer structure during summer haze in Beijing, Atmos. Environ., 74, 413-421, 10.1016/j.atmosenv.2013.03.011, 2013.
Tie, X., Huang, R.-J., Cao, J., Zhang, Q., Cheng, Y., Su, H., Chang, D., Pöschl, U., Hoffmann, T., Dusek, U., Li, G., Worsnop, D. R., and O'Dowd, C. D.: Severe Pollution in China Amplified by Atmospheric Moisture, Sci. Rep., 7, 15760, https://doi.org/10.1038/s41598-017-15909-1, 2017.
Tucker, S. C., Senff, C. J., Weickmann, A. M., Brewer, W. A., Banta, R. M., Sandberg, S. P., Law, D. C., Hardesty, R. M.: Doppler lidar estimation of mixing height using turbulence, shear, and aerosol profiles, J. Atmos. Ocean. Technol., 26(4): 673-688, 2009.
Van Den Heever, S. C., and Cotton, W. R.: Urban aerosol impacts on downwind convective storms, J. Appl. Meteorol. Climatol., 46, 828-850, 10.1175/jam2492.1, 2007.
Vautard R., Cattiaux J., Yiou P., Th´epaut J-N and Ciais P.: Northern Hemisphere atmospheric stilling partly attributed to an increase in surface roughness Nat. Geosci. 3, 756–761, 2010.
Wang, J. D., Xing, J., Wang, S. X., and Hao, J. M.: The pathway of aerosol direct effects impact on air quality: a case study by using process analysis. In EGU General Assembly Conference Abstracts, 19, 8568, 2017.
Wang, L. L., Li, D., Gao, Z. Q., Sun, T., Guo, X. F., and Bou-Zeid, E.: Turbulent transport of momentum and scalars above an urban canopy, Boundary-Layer Meteorol., 150, 485-511, 10.1007/s10546-013-9877-z, 2014.
Wang, L. T., Wei, Z., Yang, J., Zhang, Y., Zhang, F. F., Su, J., Meng, C. C., and Zhang, Q.: The 2013 severe haze over southern Hebei, China: model evaluation, source apportionment, and policy implications, Atmos. Chem. Phys., 14, 3151-3173, 10.5194/acp-14-3151-2014, 2014.
Wang, L., Wang, H., Liu, J., Gao, Z., Yang, Y., Zhang, X., Li, Y. and Huang, M.: Impacts of the near-surface urban boundary layer structure on PM2.5 concentrations in Beijing during winter. Sci Total Environ 669: 493-504, 10.5194/acp-2018-1184, 2018.
Wang, X. R., Miao, S. G., Dou, J. X., Dong, P., and Wang, J. L.: Observation and analysis of the air pollution impacts on radiation balance of urban and suburb areas in Beijing, Chinese J. Geophys. (in Chinese), 59(11), 3996-4006, 10.6038/cjg20161106, 2016.
Wang, Y., Li, Z. Q., Zhang, Y., Wang, Q., and Ma, J. Z.: Impact of aerosols on radiation during a heavy haze event in Beijing, IOP Conf. Ser.: Earth Environ. Sci., 17, 012012, 10.1088/1755-1315/17/1/012012, 2014.
Xia, X. G., Li, Z. Q., Holben, B., Wang, P. C., Eck, T., Chen, H. B., Cribb, M., and Zhao, Y. X.: Aerosol optical properties and radiative effects in the Yangtze Delta region of China, J. Geophys. Res., 112, 10.1029/2007jd008859, 2007.
Yang Y.J., Zheng, X.Y., Gao, Z. Q., Wang, H., Wang, T.J., Li, Y.B., Lau, G.l N.C., Yim,S. H.L.: Long-Term Trends of Persistent Synoptic Circulation Events in Planetary Boundary Layer and Their Relationships with Haze Pollution in Winter

969 Half-Year over Eastern China, J. Geophys. Res.,doi: 10.1029/2018JD028982, 2018
970 Yang, T., Gbaguidi, A., Zhang, W., Wang, X. Q., Wang, Z. F. and Yan, P. :
971 Model-Integration of Anthropogenic Heat for Improving Air Quality Forecasts over
972 the Beijing Megacity. Aerosol Air Qual.Res., 18(3), 790-802,
973 10.4209/aaqr.2017.04.0155. 2017.
974 Yang, T., Wang, Z. F., Zhang, W., Gbaguidi, A., Sugimoto, N., Wang, X. Q., Matsui, I.,
975 and Sun, Y. L.: Technical note: Boundary layer height determination from lidar for
976 improving air pollution episode modeling: development of new algorithm and
977 evaluation, Atmos. Chem. Phys., 17, 6215-6225, 10.5194/acp-17-6215-2017, 2017.
978 Ye, X. X., Song, Y., Cai, X. H., and Zhang, H. S.: Study on the synoptic flow patterns
979 and boundary layer process of the severe haze events over the North China Plain in
980 January 2013, Atmos. Environ., 124, 129-145, 10.1016/j.atmosenv.2015.06.011, 2016.
981 Yu, H. B., Liu, S. C., and Dickinson, R. E.: Radiative effects of aerosols on the
982 evolution of the atmospheric boundary layer, J. Geophys. Res., 107,
983 10.1029/2001jd000754, 2002.
984 Yu, M., Carmichael, G.R., Zhu, T. and Cheng, Y. F.: Sensitivity of predicted pollutant
985 levels to anthropogenic heat emissions in Beijing. Atmos. Environ., 89: 169-178,
986 10.1016/j.atmosenv.2014.01.034,2014.
987 Zhang, R. H., Li, Q., and Zhang, R. N.: Meteorological conditions for the persistent
988 severe fog and haze event over eastern China in January 2013, Science China Earth
989 Sciences, 57, 26-35, 10.1007/s11430-013-4774-3, 2014.
990 Zhang, X. Y., Sun, J. Y., Wang, Y. Q., Li, W. J., Zhang, Q., Wang, W. G., Quan, J. N.,
991 Cao, G. L., Wang, J. Z., Yang, Y. Q., and Zhang, Y. M.: Factors contributing to haze
992 and fog in china. Chin. Sci. Bull., 58(13), 1178, doi: 10.1360/972013-150, 2013.
993 Zhang, X. Y., Zhong, J. T., Wang, J. Z., Wang, Y. Q., and Liu, Y. J.: The interdecadal
994 worsening of weather conditions affecting aerosol pollution in the Beijing area in
995 relation to climate warming. Atmos. Chem. Phys., 18, 1–9.
996 https://doi.org/10.5194/acp-18-1-2018, 2018.
997 Zhao, X. J., Zhao, P. S., Xu, J., Meng, W., Pu, W. W., Dong, F., He, D., and Shi, Q. F.:
998 Analysis of a winter regional haze event and its formation mechanism in the North
999 China Plain, Atmos. Chem. Phys., 13, 5685-5696, 10.5194/acp-13-5685-2013, 2013.
1000 Zhong, J. T., Zhang, X. Y., Wang, Y. Q., Sun, J. Y., Zhang, Y. M., Wang, J. Z., Tan, K.
1001 Y., Shen, X. J., Che, H. C., Zhang, L., Zhang, Z. X., Qi, X. F., Zhao, H. R., Ren, S. X.,
1002 and Li, Y.: Relative contributions of boundary-layer meteorological factors to the
1003 explosive growth of $PM_{2.5}$ during the red-alert heavy pollution episodes in Beijing in
1004 December 2016, J. Meteor. Res., 31, 809-819, 10.1007/s13351-017-7088-0, 2017.
1005 Zhong, J. T., Zhang, X. Y., Wang, Y. Q., Wang, J. Z.i, Shen, X. J., Zhang, H. S., Wang,
1006 T. J., Xie, Z. Q., Liu, C., Zhang, H. D., Zhao, T. L., Sun, J. Y., Fan, S. J., Gao, Z. Q.,
1007 Li, Y. B. and Wang, L. L.. The two-way feedback mechanism between unfavorable
1008 meteorological conditions and cumulative aerosol pollution in various haze regions of
1009 China, Atmos. Chem. Phys. 19(5): 3287-3306, 10.5194/acp-19-3287-2019, 2019.

1010